

Diagrammatic Multiplet-Sum Method (MSM) Density-Functional Theory (DFT): III. Inclusion of Relaxation and Application to LiH

Mark E. Casida

Laboratoire de Spectrométrie, Interactions et Chimie théorique (SITh), Département de Chimie Moléculaire (DCM, UMR CNRS/UGA 5250), Institut de Chimie Moléculaire de Grenoble (ICMG, FR2607), Université Grenoble Alpes (UGA) 301 rue de la Chimie, BP 53, F-38041 Grenoble Cedex 9, FRANCE

e-mail: mark.casida@univ-grenoble-alpes.fr

Abraham Ponra

*African Institute for Mathematical Sciences (AIMS), AIMS-Cameroon, P.O. Box 608, Limbe, CAMEROON
University of Maroua, P.O. Box 814, Maroua, CAMEROON*

e-mail: abraham.ponra@aims-cameroon.org

Gadzikano Munyuki

Department of Chemistry and Earth Sciences, Faculty of Science, University of Zimbabwe, Harare, ZIMBABWE

e-mail: gadzie@gmail.com

Bharathi Natarajan

Independent Researcher, Coimbatore, Tamil Nadu, INDIA

e-mail: phyever@gmail.com

Abstract

Ideal density-functional approximations (DFAs) should account for dynamic, static, and nondynamic correlation. While common DFAs struggle with the latter two, the Ziegler-Rauk-Baerends-Daul multiplet sum method (MSM) provides a pragmatic way to include static correlation. In this article, we use diagrammatic MSM density-functional theory (diag MSM DFT) using the two-orbital two-electron model (TOTEM) to extend MSM DFT to include nondynamic correlation without relying on symmetry arguments. Building on previous formulations [A. Ponra, C. Bakasa, A.J. Etindele, and M.E. Casida, *J. Chem. Phys.* **159**, 244306 (2023); M.E. Casida, A. Ponra, C. Bakasa, and A.J. Etindele, *J. Chem. Phys.* **162**, 144317 (2025)] that lacked relaxation effects, this article incorporates relaxation via nonorthogonal configuration interaction (NOCI). We demonstrate that this modified diag MSM DFT produces an accurate ground-state potential energy curve (PEC) for lithium hydride (LiH), even at the ionic-to-open-shell-singlet avoided crossing characterized by significant charge transfer. This encouraging result suggests that the model can be extended to (at least) other singly and multiply-bonded diatomic molecules, while providing insight into a novel way to include strong correlation in DFT.

1 Introduction

Modern density-functional theory (DFT) is an exact formalism defined upon the two Hohenberg-Kohn theorems [1] and the Kohn-Sham (KS) reformulation [2]. The exact exchange-correlation

(xc) functional $E_{xc}[\rho]$ is the target for designing density-functional approximations (DFAs). A similar statement may be made about meta generalized gradient approximations or hybrid functionals which, strictly speaking, fall into the category of generalized KS theory [3]. Both in the original and in the generalized theories, the functional E_{xc} is a complicated beast, containing information about the difference between the kinetic energy of the real interacting system of electrons and the fictitious KS system of noninteracting electrons, exchange, and correlation. Electron correlation may be classified in a somewhat fuzzy, albeit useful manner, as dynamic, static, and nondynamic [4]. Dynamic correlation applies when a single determinant (SDET) is a good first approximation to the interacting wave function. Static (degenerate) correlation arises due to degeneracies among SDET states which normally implies the presence of symmetry. Nondynamic (quasidegenerate) correlation arises due to quasidegenerate states and is often associated with bond making and bond breaking. Evidently, *getting nondynamic correlation right is very important for studying chemical reactions*. Both static and nondynamic correlation constitute examples of strong correlation. These are known to show up as a particle number derivative discontinuity in E_{xc} [5, 6] and, in the exact xc potential, $v_{xc}[\rho](1) = \delta E_{xc}[\rho]/\delta\rho(1)$ as peculiar plateaus around atoms and peaks between atoms when bonds dissociate [7, 8, 9]. Such features are generally absent in commonly used DFAs and will be very difficult to include when designing better DFAs. However commonly used DFAs are known to do a good job at describing dynamic correlation, but not strong correlation. Problems show up in the form of symmetry breaking which leads to triplet instabilities when calculating excitation energies using response theory (see, e.g., Ref. [10]) and in the lowest unoccupied molecular orbital (LUMO or L) falling lower in energy than the highest occupied molecular orbital (HOMO or H) energy (see, e.g., Ref. [11]). Our idea is to extend further some classic physical approaches in DFT to include strong correlation beyond what these methods have been able to do so far. Our strategy is to learn from simple molecules and then to gradually extend our ideas to more and more complicated cases. Our hope is to keep the evolving method as simple as possible for as long as we can during the development process, while simultaneously attaining quantitative results.

It seems appropriate in a volume honoring Axel Becke, to mention that Axel once said that, “The focus of ground-state DFA developers has shifted to [what he hoped] is the last frontier, ‘strong’ correlation” [12]. Axel advocated approaching strong correlation in a very different way than we are proposing here. Axel’s preference was to try to find ways to include strong correlation through increasingly accurate xc holes. Our approach is philosophically closer to when Axel writes in the same article that, “The ultimate conclusion of combining DFT and [wave function theory] is what Bartlett calls [13] ‘*ab initio* DFT,’ a mathematical and theoretical framework that exploits the best of both worlds and seeks a systematic route to improving both.” This systematic route can be very complicated and, at least for now, we are trying to keep our approach as simple as possible, even if there are definite philosophical overlaps with Bartlett’s approach. In fact, a major point for us is to build practical experience with combining DFT and wave function theory ideas, first for simple systems, and then for increasingly complicated systems.

In the late 1970s, Ziegler, Rauk, and Baerends introduced the multiplet sum method (MSM) to add static correlation into DFT in an approximate way on the basis of a zero-order guess for the wave function [14], and this method continues to be widely used in DFT for estimating the energy of the lowest open-shell singlet state by using spin symmetry. Spatial symmetry may also be used [15, 16]. It is important to understand that MSM-DFT is *not* a route towards better DFAs, but rather is a way to profit from the strengths of existant DFAs while still including strong correlation. The strength of MSM-DFT is in its simplicity and ease of use, but it does not describe nondynamic correlation. Diagrammatic (diag) MSM-DFT was introduced recently as a way to make educated guesses of DFT matrix elements in a small configuration interaction (CI) problem (Article I [17] and

Article **II** [18]). It is important to understand that here, as in most CI calculations, the emphasis is on the quality of the energy of the lowest energy state with the introduction of “excited states” as a way to improve the lowest energy state. Nevertheless excited- and ground-states interact via avoided crossings and conical intersections, so we also find it interesting to examine the behavior of the excited-state solutions from our diag MSM DFT calculations. So far, emphasis has been on the two-level two-electron model (TOTEM). Article **II** showed promising results for calculating off-diagonal coupling elements key for describing the $[\text{Li}^+ \text{H}^-]/[\text{Li}\uparrow \text{H}\downarrow \leftrightarrow \text{Li}\downarrow \text{H}\uparrow]$ avoided crossing but also made it clear that the method is not yet quantitative. One problem with the diag MSM DFT description of the TOTEM is that it needs to include orbital relaxation effects in order to keep the CI expansion as small as possible. In the present article, we gradually add this missing relaxation through the use of configuration state functions (CSFs) built from different relaxed molecular orbitals (MOs). Many variants on our basic model have been tested but only the most useful is presented as well as some of the intermediate results that have helped us to understand how the different variants behave.

This article is organized as follows: The next section (Sec. 2) presents our choice of comparison data and discusses the principle features of the avoided crossings seen in the PECs of LiH. The chemical physics would seem to be adequately understood that we should be able to build a simple hybrid DFT/wave function theory (WFT) to be able to describe the lowest energy singlet PEC (i.e., for the $X^1\Sigma$ state). Section 3 provides a brief review of diag MSM MDFT in order to keep the present article relatively self contained. The new theory tested in the present article is the nonorthogonal configuration interaction (NOCI) method using relaxed orbitals presented in Sec. 4. Results are given in Sec. 5 and the concluding discussion is given in Sec. 6. Additional information about author contributions, computational details, and a discussion of the origin of a key approximation made in the present work may be found in the supplementary information (SI).

2 Comparison Data

Comparisons will be made against the same high-quality LiH PECs [19] as in Articles **I** and **II** which we will label as EXACT. “Exact” is, of course, a relative term, but these EXACT curves are essentially exact with respect to our model calculations and so provide an excellent comparison.

Lithium hydride is analogous to sodium hydride (Na^+H^-), a well-known reagent in organic chemistry. It is ionically bonded at its equilibrium geometry but dissociates to the neutral atoms in the gas phase because of a series of avoided crossings. These avoided crossings are nicely shown in **Fig. 1**. The $\text{Li}^+ + \text{H}^-$ diabatic curve crosses the curves that correspond to the Heitler-London valence-bond (VB) description of covalent bonding $[\text{Li-H}] = [\text{Li}\uparrow \text{H}\downarrow \leftrightarrow \text{Li}\downarrow \text{H}\uparrow]$ where H dissociates to its ground state but Li is in an excited state. [We will often indicate Lewis dot structures (LDS) by square brackets when additional clarity seems desirable.]

The present article focuses on the region $2.1 \text{ bohr} < R < 10.0 \text{ bohr}$ shown in **Fig. 2** and, in particular, on the $[\text{Li}^+ + \text{H}^-]/[\text{Li}(2s) + \text{H}(1s)]$ ($X^1\Sigma/A^1\Sigma$) avoided crossing. However it is clear that there is also a contribution from the $[\text{Li}^+ + \text{H}^-]/[\text{Li}(2p) + \text{H}(1s)]$ ($A^1\Sigma/C^1\Sigma$) near 10 bohr. As seen in Fig. 3 of Article **II**, the Coulson-Fischer point where the different-orbitals-for-different-spins (DODS) calculation falls below the same-orbitals-for-different-spins (SODS) calculation is at about 6.1 bohr which is (not unexpectedly) also very close to where the $[\text{Li}^+ + \text{H}^-]/[\text{Li}(2s) + \text{H}(1s)]$ diabatic curves cross.

Although not exact, this is an appropriate place to introduce the TOTEM that we have used in Articles **I** and **II** and which is used in the present article. The most important and difficult aspect of any multideterminant (MDET) approach is the choice of an orbital reference space. This is

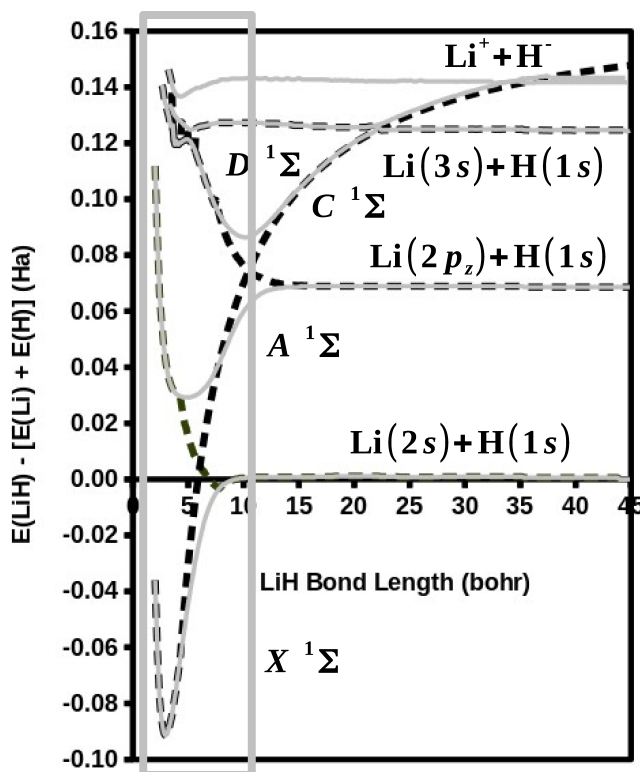


Figure 1: EXACT singlet PECs for LiH. The grey adiabatic curves were digitized from Fig. 1 of Ref. [19] using WEBPLOTDIGITIZER [20]. The adiabatic curve labels $X^1\Sigma$, $A^1\Sigma$, $C^1\Sigma$, and $D^1\Sigma$ are traditional. The dashed black curves are rough diabatic curves more or less constructed by hand. A notable exception is the $\text{Li}^+ + \text{H}^-$ diabatic curve which has the form $E - 1/R$ where R is the LiH bond distance and $E = 0.17$ Ha and which provides a very nice and rigorous diabatic curve over a large range of R . The value E is close to the expected value, which is the energy needed to transfer an electron $\text{Li} + \text{H} \rightarrow \text{Li}^- + \text{H}^+$ at infinite R . Specifically, $E = \text{IP}(\text{Li}) - \text{EA}(\text{H}) = 0.20$ Ha using the known ionization potential (IP) of the lithium atom and the known electron affinity (EA) of the hydrogen atom.

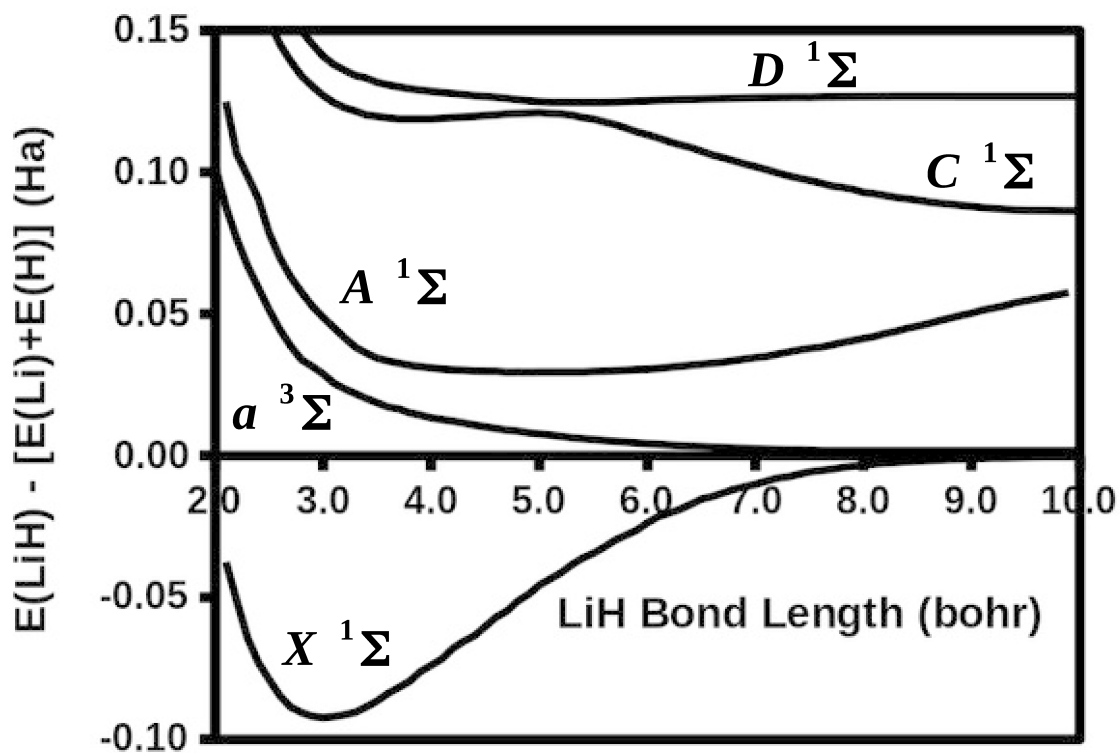


Figure 2: EXACT PECs for LiH from Ref. [19], including the lowest triplet PEC. (Small wiggles in the curves are from the digitization process using WEBPLOTDIGITIZER [20].) Note that the important $A^1\Sigma$ state was inadvertently omitted from the corresponding figures in Articles I and II.

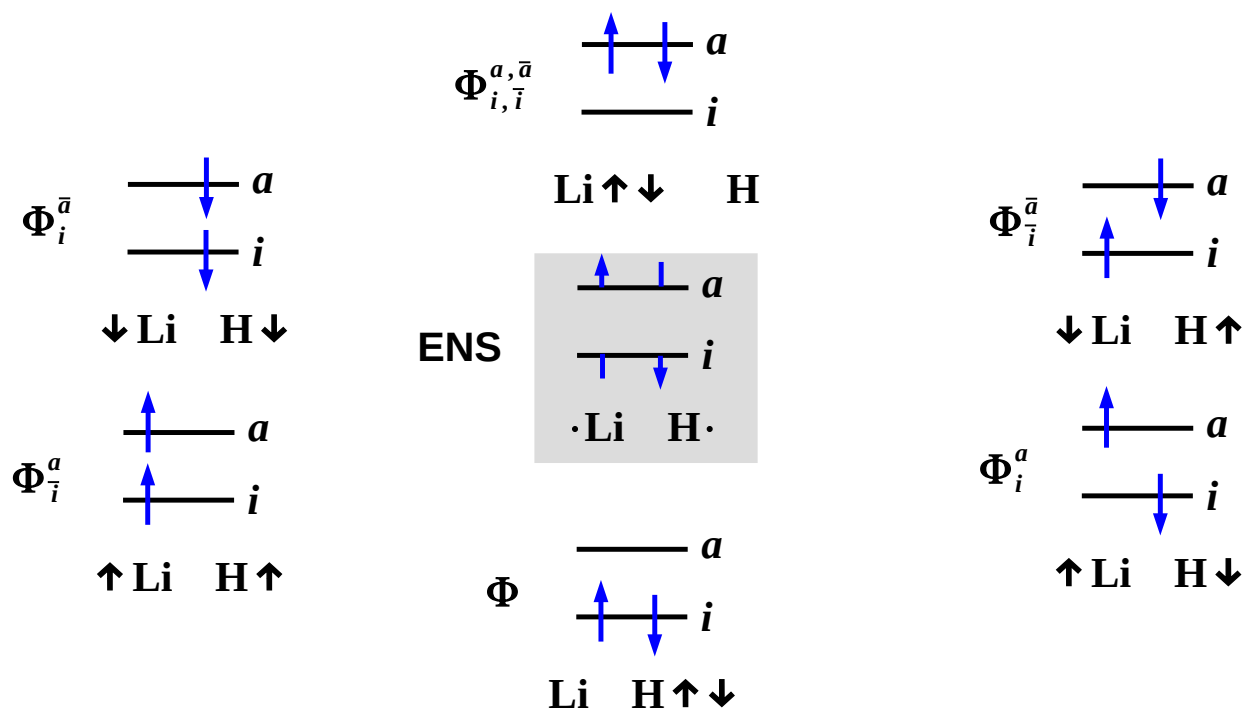


Figure 3: Two-level two-electron model (TOTEM) of LiH. Here $\Phi = |i, \bar{i}|$ is a single determinant and $\Phi_{i,j,\dots}^{a,b,\dots} = \dots b^\dagger j a^\dagger i \Phi$ is an excited determinant. The Lewis dot structures (LDS) are only intended to be suggestive as the spins can delocalize onto both atoms.

Number	Function
Single Determinantal	
1	$\Phi_0 = \Phi = \Phi_{\text{GS}}$
2	$\Phi_M = \Phi_i^a = \Phi_{\text{MIX}}$
3	$\Phi_{\bar{M}} = \Phi_i^{\bar{a}}$
4	$\Phi_D = \Phi_{i,i}^{a,\bar{a}} = \Phi_{\text{DEX}}$
Triplet CSF	
	$\Phi_T = (1/\sqrt{2})(\Phi_i^{\bar{a}} - \Phi_i^a)$
Singlet CSFs	
1	$\Phi_0 = \Phi = \Phi_{\text{GS}}$
2	$\Phi_S = (1/\sqrt{2})(\Phi_i^{\bar{a}} + \Phi_i^a) = \Phi_{\text{OSS}}$
3	$\Phi_D = \Phi_{i,i}^{a,\bar{a}} = \Phi_{\text{DEX}}$

Table 1: Single-determinantal and spin-adapted 2-electron configuration state functions (CSFs) for $M_S = 0$. See also Fig. 3. GS stands for the “ground-state” SDET; T is the triplet CSF; MIX is a mixed-symmetry SDET; OSS is the “open-shell singlet” CSF; and DEX is the “doubly-excited” SDET.

where “chemical intuition” (i.e., historical and personal practical experience) intervenes. The usual textbook molecular orbital (MO) diagram for LiH involves a HOMO bonding combination that is mostly located on the H but has some component on Li and a LUMO antibonding combination that is mostly located on the Li but has some component on H (see the SI of Article **I**). This is confirmed by MOLDEEN [21] images of these orbitals shown in Article **II** and in the corresponding SI. This gives us the TOTEM model illustrated in **Fig. 3**. *A priori* this allows us to describe the $[\text{Li}(2s) + \text{H}(1s)]$ and $[\text{Li}^+ + \text{H}^-]$ diabatic curves, which should be enough to describe the avoided crossing of principal interest (but not the $[\text{Li}^+ + \text{H}^-]/[\text{Li}(2p_z) + \text{H}(1s)]$ avoided crossing!) The question also arises in this particular TOTEM as to the energy of the doubly excited $[\text{Li}^- + \text{H}^+]$ state. In the asymptotic (large R) limit, we expect an energy equal to $\text{IP}(\text{H}) - \text{EA}(\text{Li}) = 0.48$ Ha on the basis of experimental values. For comparison, the relaxed energy at $R = 10.0$ bohr of the doubly excited SDET is 0.35 Ha. This is an important number to keep in mind when examining the results of our calculations.

3 Diagrammatic MSM-DFT

This section primarily contains provides a brief review in order to keep the present work as self-contained as possible. The basic idea for diagrammatic MSM-DFT has already been presented in Article **I** and was completed—except for relaxation—in Article **II** for the TOTEM. Here we give a minimum of review and describe how relaxation is to be included. Since our ultimate objective (which is beyond the scope of this article) is to get excited states by doing response theory on the ground state (GS), and because symmetry breaking is known to lead to triplet instabilities in response theory, we insist upon using a SODS theory.

All of the work up to this point has assumed a single set of MOs obtained from some single reference (REF) calculation. We will return to this choice of REF later. For now, let us assume that this has already been done. We first consider all the determinants with $M_S = 0$ and then make the spin-symmetry adapted CSFs whose labelling is given in **Table 1**. The triplet state energy is,

$$E_T^{\text{REF}} = E_{KS}[\Phi_i^a], \quad (1)$$

Article	
I [17]	Determination of A via MSM-DFT and of B via diag MSM-DFT
II [18]	Determination of C and D via diag MSM-DFT
III	Present work

Table 2: Summary of key articles in diag MSM-DFT.

where we have expressed the KS energy as a functional of the KS SDET wave function, in this case Φ_i^a constructed from the REF MOs. The MSM singlet wave function has the form,

$$\Psi = C_{\text{GS}}\Phi_{\text{GS}}^{\text{REF}} + C_{\text{OSS}}\Phi_{\text{OSS}}^{\text{REF}} + C_{\text{DEX}}\Phi_{\text{DEX}}^{\text{REF}}, \quad (2)$$

which leads to the small CI equation,

$$\begin{bmatrix} E_0^{\text{REF}} & \sqrt{2}D & B \\ \sqrt{2}D & E_M^{\text{REF}} + A & \sqrt{2}C \\ B & \sqrt{2}C & E_D^{\text{REF}} \end{bmatrix} \begin{pmatrix} C_{\text{GS}} \\ C_{\text{OSS}} \\ C_{\text{DEX}} \end{pmatrix} = E \begin{pmatrix} C_{\text{GS}} \\ C_{\text{OSS}} \\ C_{\text{DEX}} \end{pmatrix}. \quad (3)$$

The matrix elements A , B , C , and D were derived in previous articles (**Table 2**) but are reviewed here for the sake of completeness. In Eq. (3), $\Phi_{\text{GS}} = \Phi_0$ designates the ground-state (GS) SDET, $\Phi_{\text{OSS}} = \Phi_S$ designates the open-shell singlet (OSS) CSF, and $\Phi_{\text{DEX}} = \Phi_D$ designates the doubly-excited (DEX) SDET. The SDET energies are calculated as,

$$E_0^{\text{REF}} = E[\Phi_0], \quad E_M^{\text{REF}} = E[\Phi_M] = E[\Phi_{\bar{M}}], \quad E_D^{\text{REF}} = E[\Phi_D], \quad (4)$$

using the REF MOs. Following Ref. [14],

$$A = E_M^{\text{REF}} - E_T^{\text{REF}}. \quad (5)$$

From Article **I**,

$$B = A. \quad (6)$$

How C and D are calculated depends upon the choice of REF.

Both Articles **I** and **II** used a REF calculation with half an electron of each spin in orbitals i and a . This choice was made, in part, to minimize symmetry breaking so that we could work with SODS orbitals. We will refer to this as the ensemble (ENS) reference as the density matrix may be obtained by constructing a two-electron ENS in various ways and then forming the corresponding one-electron reduced density matrix,

$$\begin{aligned} \hat{\gamma}_{\text{ENS}} &= \frac{1}{2} (|i\rangle\langle i| + |\bar{i}\rangle\langle \bar{i}| + |a\rangle\langle a| + |\bar{a}\rangle\langle \bar{a}|) \\ &= \frac{1}{4} (\hat{\gamma}_0 + \hat{\gamma}_S + \hat{\gamma}_T + \hat{\gamma}_D) \\ &= \frac{1}{2} (\hat{\gamma}_0 + \hat{\gamma}_D) \\ &= \frac{1}{2} (\hat{\gamma}_M + \hat{\gamma}_{\bar{M}}) = \frac{1}{2} (\hat{\gamma}_S + \hat{\gamma}_T) \\ &= \hat{\gamma}_S = \hat{\gamma}_T. \end{aligned} \quad (7)$$

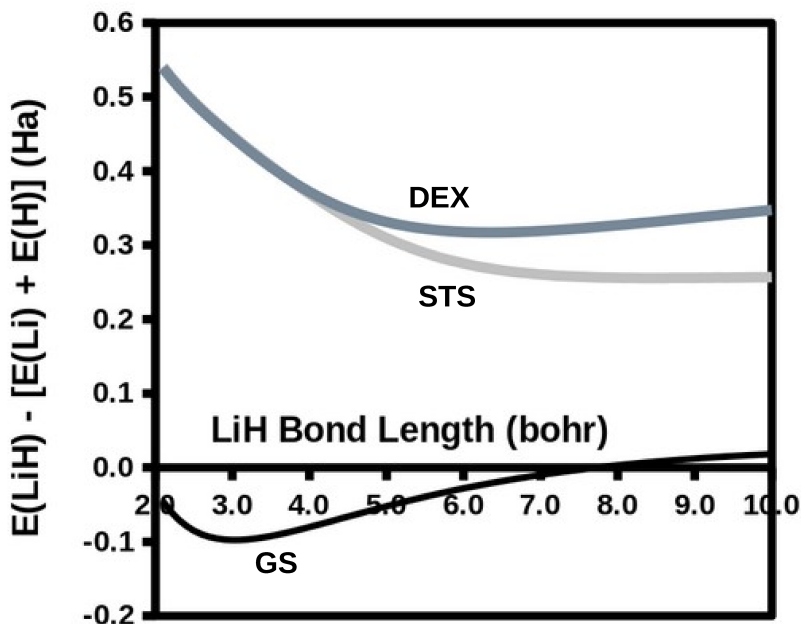


Figure 4: Relaxed GS SDET PEC, relaxed DEX SDET PEC, and a PEC obtained by adding Slater’s transition state (STS) excitation energy to the relaxed GS SDET PEC.

We may now specify more clearly that we will always be taking,

$$B = A = E_M^{\text{ENS}} - E_T^{\text{ENS}}. \quad (8)$$

Each line provides a different justification for choosing $\text{REF} = \text{ENS}$. For example, line 2 of Eq. (7) tries to be unbiased. Line 3 of Eq. (7) suggests that a compromise is being made between the ground and doubly-excited CSF. Line 4 of Eq. (7) indicates that this is an especially good choice for describing the mixed-symmetry or triplet-and-open-shell space. Line 5 of Eq. (7) further emphasizes that these orbitals are a good choice for either the triplet or the open-shell energy calculation. This was indeed found for the triplet state in Articles **I** and **II**.

Perhaps just as importantly is the fact that occupying the LUMO gives it some *physical meaning* that might otherwise be absent. Axel Becke called this the OOO principle, for “occupied orbitals only” [12]. Such physical meaning is important when trying to construct compact wave function representations. In particular, exciting half an electron of each spin from the HOMO to the LUMO is exactly Slater’s transition state (STS) for the $\text{HOMO}^2 \rightarrow \text{LUMO}^2$ double excitation. The STS for

making a double excitation is,

$$\begin{aligned}
\Delta E_D &= E_D - E_0 \\
&= E(n_H^\alpha = 1, n_H^\beta = 1, n_L^\alpha = 0, n_L^\beta = 0) \\
&= \int_0^1 \frac{E(n_H^\alpha = \lambda, n_H^\beta = \lambda, n_L^\alpha = 1 - \lambda, n_L^\beta = 1 - \lambda)}{d\lambda} d\lambda \\
&= \int_0^1 \left(\epsilon_L^\alpha(n_H^\alpha = \lambda, n_H^\beta = \lambda, n_L^\alpha = 1 - \lambda, n_L^\beta = 1 - \lambda) \right. \\
&\quad + \epsilon_L^\beta(n_H^\alpha = \lambda, n_H^\beta = \lambda, n_L^\alpha = 1 - \lambda, n_L^\beta = 1 - \lambda) \\
&\quad - \epsilon_H^\alpha(n_H^\alpha = \lambda, n_H^\beta = \lambda, n_L^\alpha = 1 - \lambda, n_L^\beta = 1 - \lambda) \\
&\quad \left. - \epsilon_H^\beta(n_H^\alpha = \lambda, n_H^\beta = \lambda, n_L^\alpha = 1 - \lambda, n_L^\beta = 1 - \lambda) \right) d\lambda \\
&\approx 2(\epsilon_L(ENS) - \epsilon_H(ENS)) .
\end{aligned} \tag{9}$$

This is the STS line in **Fig. 4**. Also shown is the DEX PEC calculated with the variationally optimized DEX orbitals. We can calculate this because DEMON2K has a maximum-overlap orbital-following algorithm that makes sure that the correct orbitals are occupied during the iterations in order to avoid variational collapse. Nevertheless, two different SCF solutions were found and only the lowest energy one was used. This DEX PEC solution is the closest thing that we have to the exact DEX PEC. As might be expected based upon the variational principle, the DEX PEC calculated with the ENS MOs (not shown) is higher in energy but parallel to the DEX curve. Theory suggests that the STS line should be an approximation to the exact DEX PEC. As we can see, this STS approximation works well for $R < 4.0$ bohr, but thereafter is only a very rough approximation.

What about the C and D matrix elements? Article **II** postulated that

$$\begin{aligned}
C &= f_{i,a}^{\text{ENS}}[\gamma_{\text{DEX}}^{\text{ENS}}] \\
D &= f_{i,a}^{\text{ENS}}[\gamma_{\text{GS}}^{\text{ENS}}],
\end{aligned} \tag{10}$$

on the basis of similarities with wave function theory. Here $f_{i,a}^{\text{ENS}}$ is the off-diagonal element of the KS orbital hamiltonian matrix calculated in the ENS MO basis set. However this choice is not unique because another seemingly logical choice for the reference is the GS. For the C and D matrix elements (temporarily denoted as \tilde{C} and \tilde{D} for consistency with the SI),

$$\begin{aligned}
\tilde{C} &= f_{i,a}^{\text{GS}}[\gamma_{\text{DEX}}^{\text{GS}}] \approx 2f_{i,a}^{\text{ENS}}[\gamma_{\text{DEX}}^{\text{ENS}}] = 2C \\
\tilde{D} &= f_{i,a}^{\text{GS}}[\gamma_{\text{GS}}^{\text{GS}}] = 0.
\end{aligned} \tag{11}$$

where $f_{i,a}^{\text{GS}}[\gamma_{\text{DEX}}^{\text{GS}}]$ is the off-diagonal element of the KS orbital hamiltonian matrix in the GS MO basis set calculated with the DEX matrix element constructed with DEX occupation numbers but GS MOs, $f_{i,a}^{\text{ENS}}[\gamma_{\text{DEX}}^{\text{ENS}}]$ is the off-diagonal element of the KS orbital hamiltonian matrix in the ENS MO basis set calculated with the approximate DEX density matrix constructed with DEX occupation numbers but ENS MOs, and $f_{i,a}^{\text{GS}}$ is the off-diagonal element of the KS orbital hamiltonian matrix in the GS MO basis set calculated with the GS density matrix constructed with GS occupation numbers. The second line of Eq. (11) is the Kohn-Sham equivalent of Brillouin's theorem (i.e., the Kohn-Sham orbital matrix is diagonal in the canonical Kohn-Sham orbitals). However the approximation in the first line of Eq. (11), which involves a change of reference orbitals, is a little involved to derived. It is presented diagrammatically in Article **II** [Compare Fig. 5 and Eq. (23) of Article **II**] and an explicit argument is given in the SI for the present work.

4 Diagrammatic MSM-DFT with Relaxation

This section contains the new theory studied in this article. Specifically, it was recognized in Article **II**, that the diagrammatic MSM-DFT method presented thus far is missing important relaxation effects. In principle, these can be included by using nonorthogonal configuration interaction (NOCI) where the different CSFs in the CI expansion are obtained from a different reference. *A priori*, our ideal NOCI wave function should take the form,

$$\Psi = C_{\text{GS}}\Phi_{\text{GS}}^{\text{GS}} + C_{\text{OSS}}\Phi_{\text{OSS}}^{\text{ENS}} + C_{\text{DEX}}\Phi_{\text{DEX}}^{\text{DEX}}, \quad (12)$$

where the superscripts emphasize that $\Phi_{\text{GS}}^{\text{GS}}$ is variationally optimal for the ground SDET state and $\Phi_{\text{DEX}}^{\text{DEX}}$ is variationally optimal for the doubly excited SDET state. We will keep the ENS orbitals for constructing the open-shell singlet CSF. It is actually interesting to not go immediately to three different reference states but to also look at some intermediate combinations where, say, $\Phi_{\text{OSS}}^{\text{ENS}}$ is replaced with $\Phi_{\text{OSS}}^{\text{GS}}$ as will be shown in Sec. 5.

Strictly speaking, LiH is a four-electron problem, not a two-electron problem. However there is ample experience reported in the literature that relaxation of the the doubly occupied core 1s electrons on Li may be neglected to a first approximation. This is clearly an approximation where some care is in order. In particular, care should be taken when applying the TOTEM to larger molecules with more complicated electronic configurations, such as NaF, where core relaxation may still be a reasonable approximation but where valence orbitals outside the TOTEM space are expected to show significant relaxation effects which will have to be included in our model. However, this is beyond the scope of the present work.

NOCI involves new challenges which we partially address and partially avoid in our simplified treatment. Ordinary single reference CI involves solving Eq. (3),

$$\mathbf{H}\vec{C}_I = E_I\vec{C}_I. \quad (13)$$

A multireference relaxed treatment means that there is a CSF overlap matrix \mathbf{S} which differs from unity. Its calculation is tractable because of the theorem that the overlap matrix of determinants is the determinant of the overlap matrices,

$$\langle i_1, i_2, \dots, i_N | j_1, j_2, \dots, j_N \rangle = \det \begin{vmatrix} \langle i_1 | j_1 \rangle & \langle i_1 | j_2 \rangle & \cdots & \langle i_1 | i_N \rangle \\ \langle i_2 | j_1 \rangle & \langle i_2 | j_2 \rangle & \cdots & \langle i_2 | i_N \rangle \\ \vdots & \vdots & \ddots & \vdots \\ \langle i_N | j_1 \rangle & \langle i_N | j_2 \rangle & \cdots & \langle i_N | i_N \rangle \end{vmatrix}. \quad (14)$$

The necessary overlap matrix may then be calculated as,

$$\begin{aligned} \mathbf{S} &= \begin{bmatrix} \langle \Psi_{\text{GS}}^{\text{GS}} | \Psi_{\text{GS}}^{\text{GS}} \rangle & \langle \Psi_{\text{GS}}^{\text{GS}} | \Psi_{\text{OSS}}^{\text{ENS}} \rangle & \langle \Psi_{\text{GS}}^{\text{GS}} | \Psi_{\text{DEX}}^{\text{DEX}} \rangle \\ \langle \Psi_{\text{OSS}}^{\text{ENS}} | \Psi_{\text{GS}}^{\text{GS}} \rangle & \langle \Psi_{\text{OSS}}^{\text{ENS}} | \Psi_{\text{OSS}}^{\text{ENS}} \rangle & \langle \Psi_{\text{OSS}}^{\text{ENS}} | \Psi_{\text{DEX}}^{\text{DEX}} \rangle \\ \langle \Psi_{\text{DEX}}^{\text{DEX}} | \Psi_{\text{GS}}^{\text{GS}} \rangle & \langle \Psi_{\text{DEX}}^{\text{DEX}} | \Psi_{\text{OSS}}^{\text{ENS}} \rangle & \langle \Psi_{\text{DEX}}^{\text{DEX}} | \Psi_{\text{DEX}}^{\text{DEX}} \rangle \end{bmatrix} \\ &= \begin{bmatrix} 1 & \sqrt{2}\langle i^{\text{GS}} | i^{\text{ENS}} \rangle \langle i^{\text{GS}} | a^{\text{ENS}} \rangle & \langle i^{\text{GS}} | a^{\text{DEX}} \rangle^2 \\ \sqrt{2}\langle i^{\text{ENS}} | i^{\text{GS}} \rangle \langle a^{\text{ENS}} | i^{\text{GS}} \rangle & 1 & \sqrt{2}\langle i^{\text{ENS}} | a^{\text{DEX}} \rangle \langle a^{\text{ENS}} | a^{\text{DEX}} \rangle \\ \langle a^{\text{DEX}} | i^{\text{GS}} \rangle^2 & \sqrt{2}\langle a^{\text{DEX}} | i^{\text{ENS}} \rangle \langle a^{\text{DEX}} | a^{\text{ENS}} \rangle & 1 \end{bmatrix}. \end{aligned} \quad (15)$$

Those familiar with VB theory know that the hamiltonian matrix elements will also include orbital overlaps. That is, we must solve a new problem,

$$\mathbf{H}'\vec{C}_I = E_I\mathbf{S}\vec{C}_I, \quad (16)$$

where in WFT,

$$\mathbf{H}' = \begin{bmatrix} E_0^{\text{GS}} & \sqrt{2}D & B \\ \sqrt{2}D & E_M^{\text{ENS}} + A & \sqrt{2}C \\ B & \sqrt{2}C & E_D^{\text{DEX}} \end{bmatrix}, \quad (17)$$

with

$$\begin{aligned} A &= \langle i_{\text{ENS}}, a_{\text{ENS}} | f_H | a_{\text{ENS}}, i_{\text{ENS}} \rangle \\ B &= 2 \langle i_{\text{GS}} | \hat{h} | a_{\text{DEX}} \rangle \langle i_{\text{GS}} | a_{\text{DEX}} \rangle + \langle i_{\text{GS}}, a_{\text{DEX}} | f_H | i_{\text{GS}}, a_{\text{DEX}} \rangle \\ C &= \langle a_{\text{DEX}} | \hat{h} | i_{\text{ENS}} \rangle \langle a_{\text{DEX}} | a_{\text{ENS}} \rangle + \langle a_{\text{DEX}} | \hat{h} | a_{\text{ENS}} \rangle \langle a_{\text{DEX}} | i_{\text{ENS}} \rangle + \langle a_{\text{DEX}}, i_{\text{ENS}} | f_H | a_{\text{DEX}}, a_{\text{ENS}} \rangle \\ D &= \langle i_{\text{GS}} | \hat{h} | a_{\text{ENS}} \rangle \langle i_{\text{GS}} | i_{\text{ENS}} \rangle + \langle i_{\text{GS}} | \hat{h} | i_{\text{ENS}} \rangle \langle i_{\text{GS}} | a_{\text{ENS}} \rangle + \langle i_{\text{GS}}, a_{\text{ENS}} | f_H | i_{\text{GS}}, i_{\text{ENS}} \rangle. \end{aligned} \quad (18)$$

Notice that $\mathbf{H}' \rightarrow \mathbf{H}$ in the limit of a single set of orthonormal reference orbitals because

$$\begin{aligned} A &\rightarrow \langle ia | f_H | ai \rangle \\ B &\rightarrow \langle ia | f_H | ia \rangle = A \text{ (if real orbitals)} \\ C &\rightarrow \langle a | \hat{h} | i \rangle + \langle ai | f_H | aa \rangle = f_{a,i}[\gamma_{\text{DEX}}] \\ D &\rightarrow \langle i | \hat{h} | a \rangle + \langle ia | f_H | ii \rangle = f_{i,a}[\gamma_{\text{GS}}], \end{aligned} \quad (19)$$

where $f_H = 1/r_{1,2}$ is the Hartree kernel.

Also notice how Eq. (18) is much more complicated than Eq. (19). In the first place, it involves treating one- and two-electron terms differently. That adds an additional level of complexity that we want to avoid unless it turns out to be absolutely necessary (which, of course, could be the case, but does not seem to be so for LiH). But the second reason is far more important: This is that diag MSM DFT requires us to replace some of the terms with xc-terms (energies or potentials) which will have to be evaluated at a specific density. The above formulae would lead to cross terms which should depend upon *two* reference densities or upon a transition density between two references. Some people do take this approach [22] and we find it very interesting. But our goal is to keep the present model as simple as possible. Since we want to avoid (for this article) the evaluation of overly complicated matrix-element expressions, we will make an *additional* approximation—namely that $\Phi_{\text{GS}}^{\text{GS}}$ and $\Phi_{\text{DEX}}^{\text{DEX}}$ may be expanded in terms of ENS CSFs as,

$$\begin{aligned} \vec{\Psi}' &= \vec{\Psi} \mathbf{M} \\ \vec{\Psi} &= \vec{\Psi}' (\mathbf{M}^\dagger \mathbf{M})^{-1} \mathbf{M}^\dagger, \end{aligned} \quad (20)$$

where

$$\begin{aligned} \vec{\Psi} &= (|\Psi_{\text{GS}}^{\text{ENS}}\rangle \quad |\Psi_{\text{OSS}}^{\text{ENS}}\rangle \quad |\Psi_{\text{DEX}}^{\text{ENS}}\rangle) \\ \vec{\Psi}' &= (|\Psi_{\text{GS}}^{\text{GS}}\rangle \quad |\Psi_{\text{OSS}}^{\text{ENS}}\rangle \quad |\Psi_{\text{DEX}}^{\text{DEX}}\rangle) \end{aligned} \quad (21)$$

and

$$\mathbf{M} = \vec{\Psi}'^\dagger \vec{\Psi}. \quad (22)$$

That is, we assume that the multireference linear combination of relaxed wave functions may be expanded as a linear combination of single reference unrelaxed wave functions. This results in a sort of projection of \mathbf{H} onto \mathbf{H}' ,

$$\begin{aligned} \mathbf{H} &= \vec{\Psi}'^\dagger \hat{H} \vec{\Psi} \\ \mathbf{H}' &= (\vec{\Psi}')^\dagger \hat{H} \vec{\Psi}' = \mathbf{M}^\dagger \mathbf{H} \mathbf{M} \\ \mathbf{S}' &= (\vec{\Psi}')^\dagger \vec{\Psi}' = \mathbf{M}^\dagger \mathbf{M}. \end{aligned} \quad (23)$$

Coherent with this approximation is that we now have a new overlap matrix as well — namely,

$$\mathbf{S}' = (\vec{\Psi}')^\dagger \vec{\Psi}' = \mathbf{M}^\dagger \mathbf{M}. \quad (24)$$

The result,

$$\mathbf{M}^\dagger \mathbf{H} \mathbf{M} \vec{C}_I = E_I \mathbf{M}^\dagger \mathbf{M} \vec{C}_I, \quad (25)$$

is rather curious because \mathbf{M}^\dagger is invertible in our calculations which leads to

$$\mathbf{H} \left(\mathbf{M} \vec{C}_I \right) = E_I \left(\mathbf{M} \vec{C}_I \right). \quad (26)$$

Since this is practically the same as our original single-reference CI equation [Eq. (13)], we may continue to solve Eq. (13) just as in Articles **I** and **II**, except that *the matrix elements of \mathbf{H} are evaluated using different relaxed reference states!* Our wave function interpretation will be based upon

$$\vec{C}'_I = \mathbf{M} \vec{C}_I. \quad (27)$$

We have seen that \mathbf{M} basically cancels out, but nevertheless enters into the theory. It can be calculated as

$$\begin{aligned} \mathbf{M} &= \begin{bmatrix} \langle \Psi_{\text{GS}}^{\text{ENS}} | \Psi_{\text{GS}}^{\text{GS}} \rangle & \langle \Psi_{\text{GS}}^{\text{ENS}} | \Psi_{\text{OSS}}^{\text{ENS}} \rangle & \langle \Psi_{\text{GS}}^{\text{ENS}} | \Psi_{\text{DEX}}^{\text{DEX}} \rangle \\ \langle \Psi_{\text{OSS}}^{\text{ENS}} | \Psi_{\text{GS}}^{\text{GS}} \rangle & \langle \Psi_{\text{OSS}}^{\text{ENS}} | \Psi_{\text{OSS}}^{\text{ENS}} \rangle & \langle \Psi_{\text{OSS}}^{\text{ENS}} | \Psi_{\text{DEX}}^{\text{DEX}} \rangle \\ \langle \Psi_{\text{DEX}}^{\text{ENS}} | \Psi_{\text{GS}}^{\text{GS}} \rangle & \langle \Psi_{\text{DEX}}^{\text{ENS}} | \Psi_{\text{OSS}}^{\text{ENS}} \rangle & \langle \Psi_{\text{DEX}}^{\text{ENS}} | \Psi_{\text{DEX}}^{\text{DEX}} \rangle \end{bmatrix} \\ &= \begin{bmatrix} \langle i^{\text{GS}} | i^{\text{ENS}} \rangle^2 & 0 & \langle i^{\text{ENS}} | a^{\text{DEX}} \rangle^2 \\ \sqrt{2} \langle i^{\text{ENS}} | i^{\text{GS}} \rangle \langle a^{\text{ENS}} | i^{\text{GS}} \rangle & 1 & \sqrt{2} \langle i^{\text{ENS}} | a^{\text{DEX}} \rangle \langle a^{\text{ENS}} | a^{\text{DEX}} \rangle \\ \langle a^{\text{ENS}} | i^{\text{GS}} \rangle^2 & 0 & \langle a^{\text{ENS}} | a^{\text{DEX}} \rangle^2 \end{bmatrix}. \end{aligned} \quad (28)$$

The matrix elements of \mathbf{M} are shown in **Fig. 5**. Critically $\langle a_{(\text{DEX})} | i_{(\text{ENS})} \rangle \approx -\langle a_{(\text{ENS})} | i_{(\text{GS})} \rangle$ which leads to $M(2, 3) \approx -M(2, 1)$. This will have consequences.

Of more interest is to calculate,

$$\mathbf{S}' = \begin{bmatrix} \langle i^{\text{GS}} | \hat{P}_{\text{MO}}^{\text{ENS}} | i^{\text{GS}} \rangle^2 & \sqrt{2} \langle i^{\text{GS}} | i^{\text{ENS}} \rangle \langle i^{\text{GS}} | a^{\text{ENS}} \rangle & \langle i^{\text{GS}} | \hat{P}_{\text{MO}}^{\text{ENS}} | a^{\text{DEX}} \rangle^2 \\ \sqrt{2} \langle i^{\text{ENS}} | i^{\text{GS}} \rangle \langle a^{\text{ENS}} | i^{\text{GS}} \rangle & 1 & \sqrt{2} \langle i^{\text{ENS}} | a^{\text{DEX}} \rangle \langle a^{\text{ENS}} | a^{\text{DEX}} \rangle \\ \langle a^{\text{DEX}} | \hat{P}_{\text{MO}}^{\text{ENS}} | i^{\text{GS}} \rangle^2 & \sqrt{2} \langle a^{\text{DEX}} | i^{\text{ENS}} \rangle \langle a^{\text{DEX}} | a^{\text{ENS}} \rangle & \langle a^{\text{DEX}} | \hat{P}_{\text{MO}}^{\text{ENS}} | a^{\text{DEX}} \rangle^2 \end{bmatrix}, \quad (29)$$

whose relation to \mathbf{S} is made clear by the use of

$$\hat{P}_{\text{MO}}^{\text{ENS}} = |i^{\text{ENS}}\rangle \langle i^{\text{ENS}}| + |a^{\text{ENS}}\rangle \langle a^{\text{ENS}}|, \quad (30)$$

which is the projection onto the ENS MO space. Replacing this projection operator with the identity operator gives the exact \mathbf{S} [Eq. (15)].

Figure 6 provides a numerical comparison of the matrix elements of \mathbf{S} and $\mathbf{S}' = \mathbf{M}^\dagger \mathbf{M}$. While there are qualitative similarities, the most unexpected aspect is that $S'(1, 3) \approx 0$ which means that the GS and the DEX are effectively decoupled in \mathbf{S}' while they are coupled in \mathbf{S} .

An even more important quantity is the lowest eigenvalue of the overlap matrix. The eigenvalues of \mathbf{S} and of \mathbf{S}' are shown in **Fig. 7(a)**. The eigenvalues of \mathbf{S}' are smaller than, but in reasonable quantitative agreement with, those of \mathbf{S} because of the formulae for the matrix elements of \mathbf{S}' contain a projection operator not found in the formulae for the matrix elements of \mathbf{S} . The eigenvalues of an overlap matrix must always be positive, unless there are linear dependencies. Such a linear dependency is developing at 10.0 bohr. For \mathbf{S} , the MO coefficients read,

$$0.504\Psi_{\text{GS}} + -0.707\Psi_{\text{OSS}} - 0.496\Psi_{\text{DEX}} \approx 0, \quad (31)$$

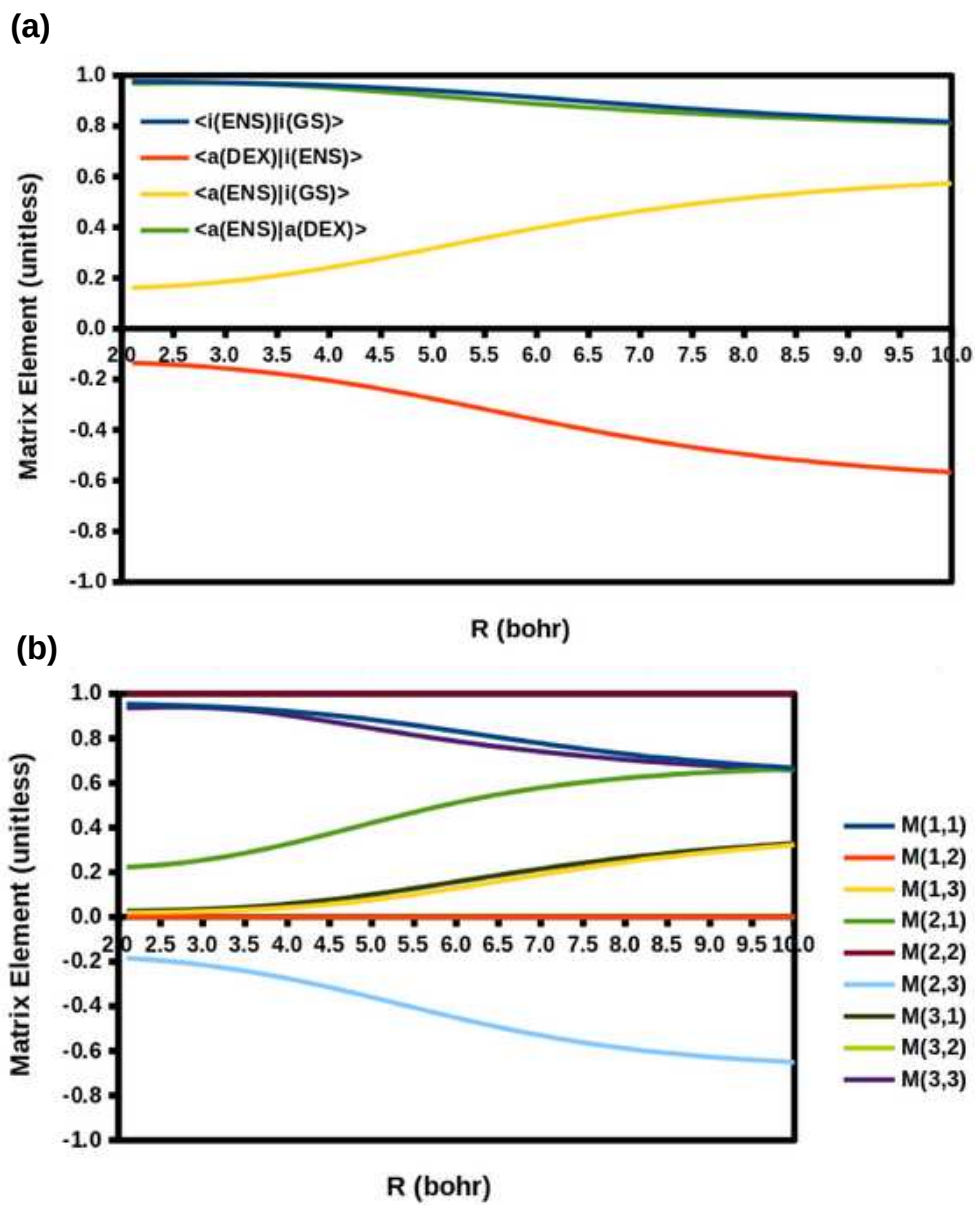


Figure 5: Matrix elements of the M (b) and the overlap elements (a) used to construct M . (See text.)

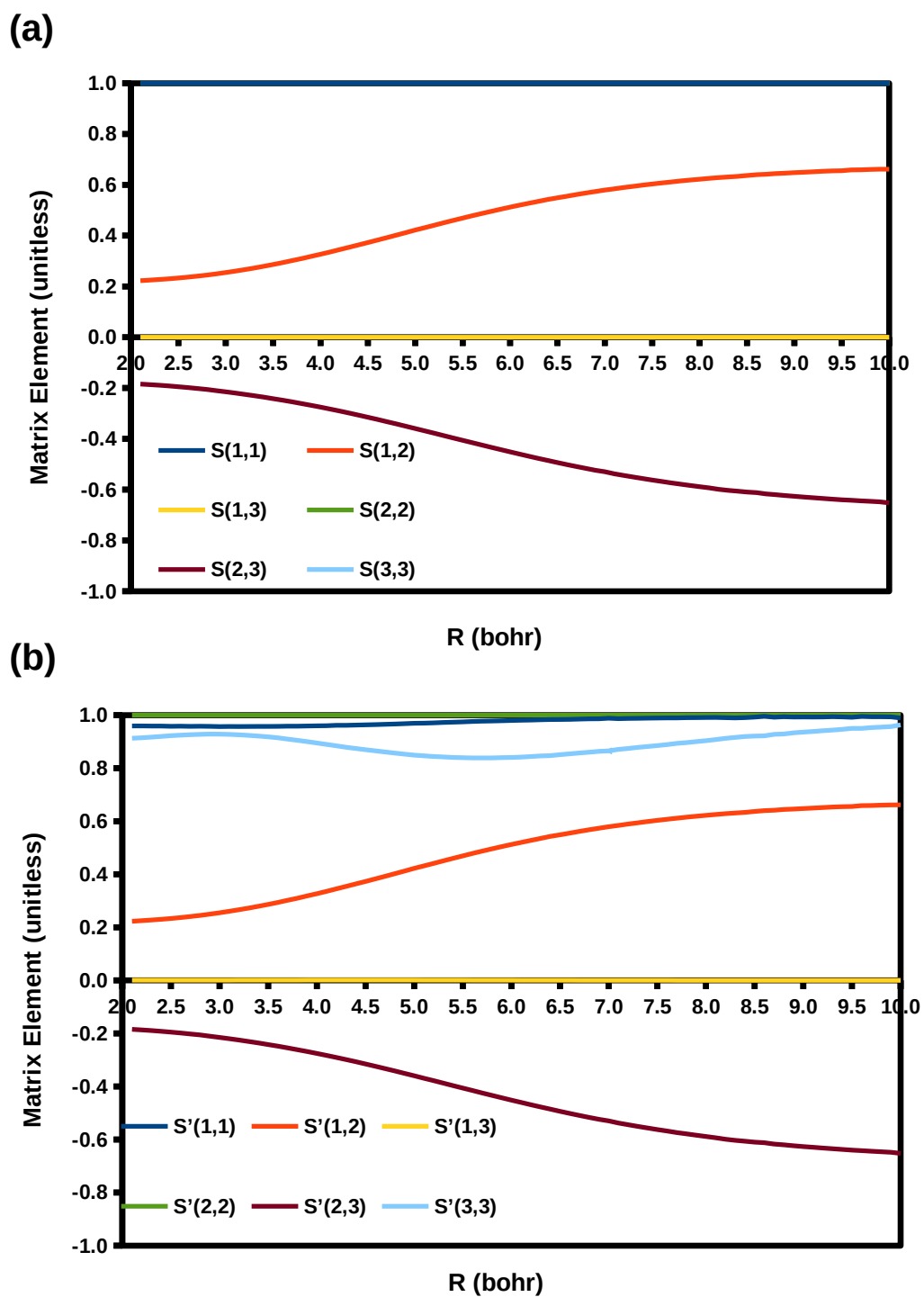


Figure 6: Matrix elements of (a) S and (b) S' (see text).

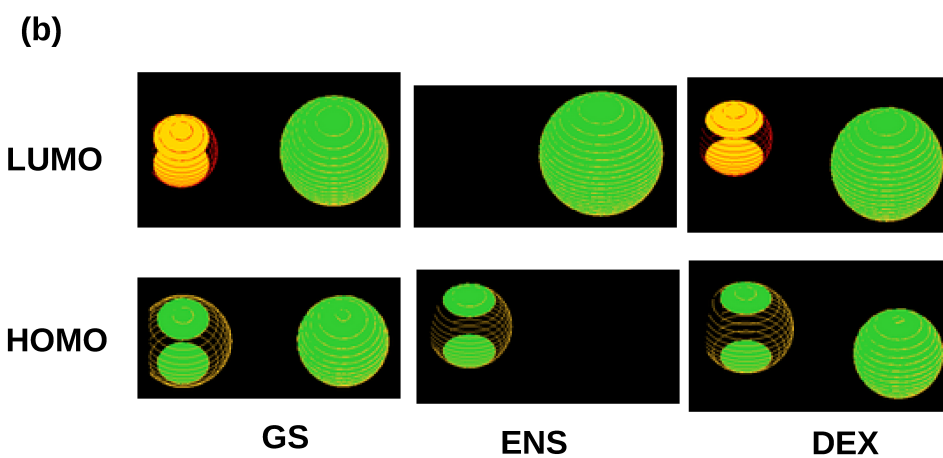
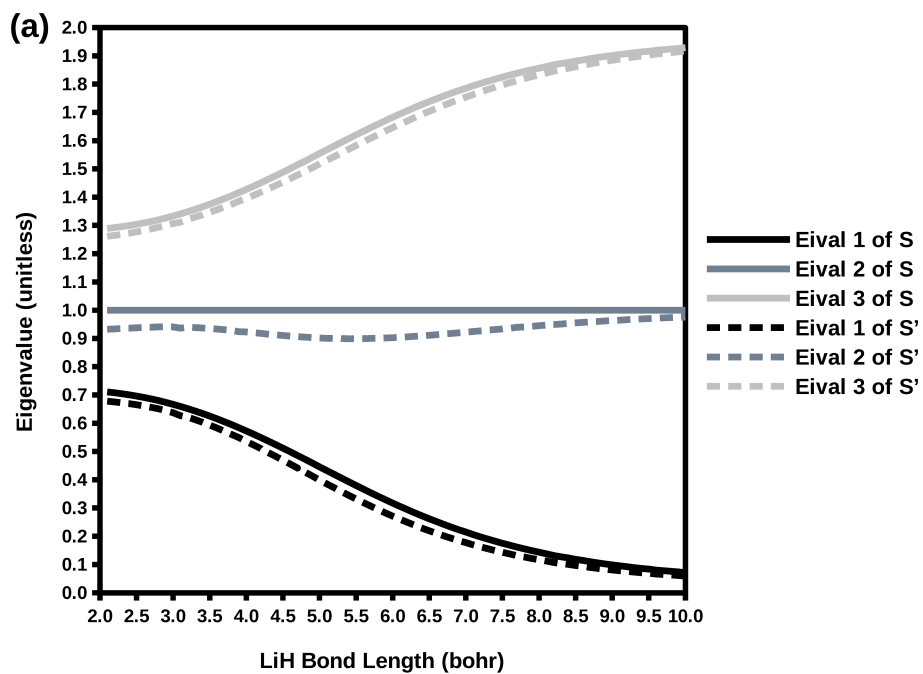


Figure 7: (a) The eigenvalues of \mathbf{S} and \mathbf{S}' as a function of bond length. (b) MOLDEEN [21] images of the HOMO and LUMO calculated for the different references with a contour value of 0.03 a.u. Note how the HOMO and LUMO of the GS and DEX SDET are bonding and antibonding combinations of similarly sized s -type orbitals while the HOMO of the ENS state is an s -type orbital localized on H and the LUMO of the ENS state is an s -type orbital localized on Li.

or

$$\frac{1}{\sqrt{2}}\Psi_{\text{OSS}} \approx \frac{1}{2}(\Psi_{\text{GS}} - \Psi_{\text{DEX}}) . \quad (32)$$

This apparently simple, and surprising, result is explained by the MOs shown in Fig. 7(b) which correspond roughly to,

$$\begin{aligned} \psi_H^{\text{GS}} &= \frac{1}{\sqrt{2}}(1s(\text{H}) + 2s(\text{Li})) \\ \psi_H^{\text{OSS}} &= 1s(\text{H}) \\ \psi_L^{\text{OSS}} &= 2s(\text{Li}) \\ \psi_L^{\text{DEX}} &= \frac{1}{\sqrt{2}}(1s(\text{H}) - 2s(\text{Li})) . \end{aligned} \quad (33)$$

From Table 1, Eq. (32) reads,

$$\frac{1}{\sqrt{2}}(|H, \bar{L}| - |L, \bar{H}|) \approx \frac{1}{2}(|H, \bar{H}| - |L, \bar{L}|) . \quad (34)$$

Inserting Eq. (33) and simplifying then gives,

$$\frac{1}{\sqrt{2}}\left(|1s(\text{H}), \overline{2s(\text{Li})}| + |2s(\text{Li}), \overline{1s(\text{H})}|\right) , \quad (35)$$

on both the left-hand and on the right-hand side of Eq. (34), thus justifying the near linear dependence of the CSFs at 10.0 bohr.

A consequence of the semi-quantitative agreement between \mathbf{S} and \mathbf{S}' is $\mathbf{H}\vec{C}_I = E_I\vec{C}_I$, $\mathbf{H}'\vec{C}_I = E_I\mathbf{S}'\vec{C}_I$, and $\mathbf{H}'\vec{C}_I = E_I\mathbf{S}\vec{C}_I$ should all produce very similar PECs. This is true for $\mathbf{H}\vec{C}_I = E_I\vec{C}_I$ and $\mathbf{H}'\vec{C}_I = E_I\mathbf{S}'\vec{C}_I$ because $\mathbf{H}'\vec{C}_I = E_I\mathbf{S}'\vec{C}_I$ is $\mathbf{M}^\dagger\mathbf{H}\mathbf{M}\vec{C}_I = \mathbf{M}^\dagger\mathbf{M}\vec{C}_I$ and \mathbf{M}^\dagger is invertible, giving $\mathbf{H}\vec{C}_I = E_I\vec{C}_I$ with $\vec{C}_I' = \mathbf{M}\vec{C}_I$. It must also be approximately true for $\mathbf{H}'\vec{C}_I = E_I\mathbf{S}\vec{C}_I$ because $\mathbf{S} \approx \mathbf{S}'$. Hence it suffices to diagonalize $\mathbf{H}''\vec{C}_I'' = E_I\vec{C}_I''$ with $\mathbf{H}'' = \mathbf{S}^{-1/2}\mathbf{H}'\mathbf{S}^{-1/2}$ and $\vec{C}_I'' = \mathbf{S}^{+1/2}\vec{C}_I'$. Our wavefunction analysis will be based directly upon \vec{C}_I , \vec{C}_I' , or \vec{C}_I'' , as appropriate, with an additional Chirgwin-Coulson analysis (see Ref. [23] and the SI) for version **v6**.

5 Results and Analysis

The aim of diag MSM DFT is to provide a tool to help find missing matrix elements for a simple hybrid of DFT for dynamic correlation and CI for static and nondynamic correlation, but it is only a tool. The diagrams in diag MSM DFT provide a basis for making educated guesses about how to calculate *appropriate* matrix elements in a small CI calculation. This is why the work reported here is exploratory in nature, just as it was in Articles **I** and **II**. We are reminded of a popular quote often attributed to Thomas Edison that reminds us that most scientific work necessarily involves a lot of trial and error, notably in the early stages: ‘‘I’ve tried everything. I have not failed. I have just found 10,000 ways that won’t work!’’ [24] The present work is no exception. Only a few of the variations tried (i.e., those shown in **Table 3**) will be discussed in order to show the systematic evolution of the theory through progressive inclusion of relaxation effects in NOCI.

The coupling matrix elements in Table 3 are shown in **Fig. 8**. They are particularly important. Matrix element D is the direct coupling between the GS CSF and the OSS CSF (GS \leftrightarrow OSS).

Variation \mathbf{v}	MOs				Coupling Matrices		Hamiltonian	Overlap
	GS	T	M	DEX	C	D		
$\mathbf{v0}$	ENS	ENS	ENS	ENS	$f_{i,a}^{\text{ENS}}[\gamma_D^{\text{ENS}}]$	$f_{i,a}^{\text{ENS}}[\gamma_0^{\text{ENS}}]$	\mathbf{H}	1
$\mathbf{v1}$	GS	GS	GS	GS	$f_{i,a}^{\text{GS}}[\gamma_D^{\text{GS}}]$	0	\mathbf{H}	1
($\mathbf{v2}$)	GS	GS	GS	GS	$2f_{i,a}^{\text{ENS}}[\gamma_D^{\text{ENS}}]$	0	\mathbf{H}	1
$\mathbf{v3}$	GS	GS	GS	DEX	$2f_{i,a}^{\text{ENS}}[\gamma_D^{\text{ENS}}]$	0	\mathbf{H}	1
$\mathbf{v4}$	GS	ENS	ENS	DEX	$f_{i,a}^{\text{ENS}}[\gamma_D^{\text{ENS}}]$	$f_{i,a}^{\text{ENS}}[\gamma_0^{\text{ENS}}]$	\mathbf{H}	1
$\mathbf{v5}$	GS	ENS	ENS	DEX	$2f_{i,a}^{\text{ENS}}[\gamma_D^{\text{ENS}}]$	0	\mathbf{H}	1
$\mathbf{v6}$	GS	ENS	ENS	DEX	$2f_{i,a}^{\text{ENS}}[\gamma_D^{\text{ENS}}]$	0	\mathbf{H}'	\mathbf{S}

Table 3: Variations tested: GS, groundstate; ENS, ensemble with half an electron of each spin in the HOMO and in the LUMO; DEX, doubly excited. Here $\mathbf{H}' = \mathbf{M}^\dagger \mathbf{H} \mathbf{M}$ and $\mathbf{S}' = \mathbf{M}^\dagger \mathbf{M}$. The variation $\mathbf{v2}$ is in parentheses as this variation is only touched upon in the text.

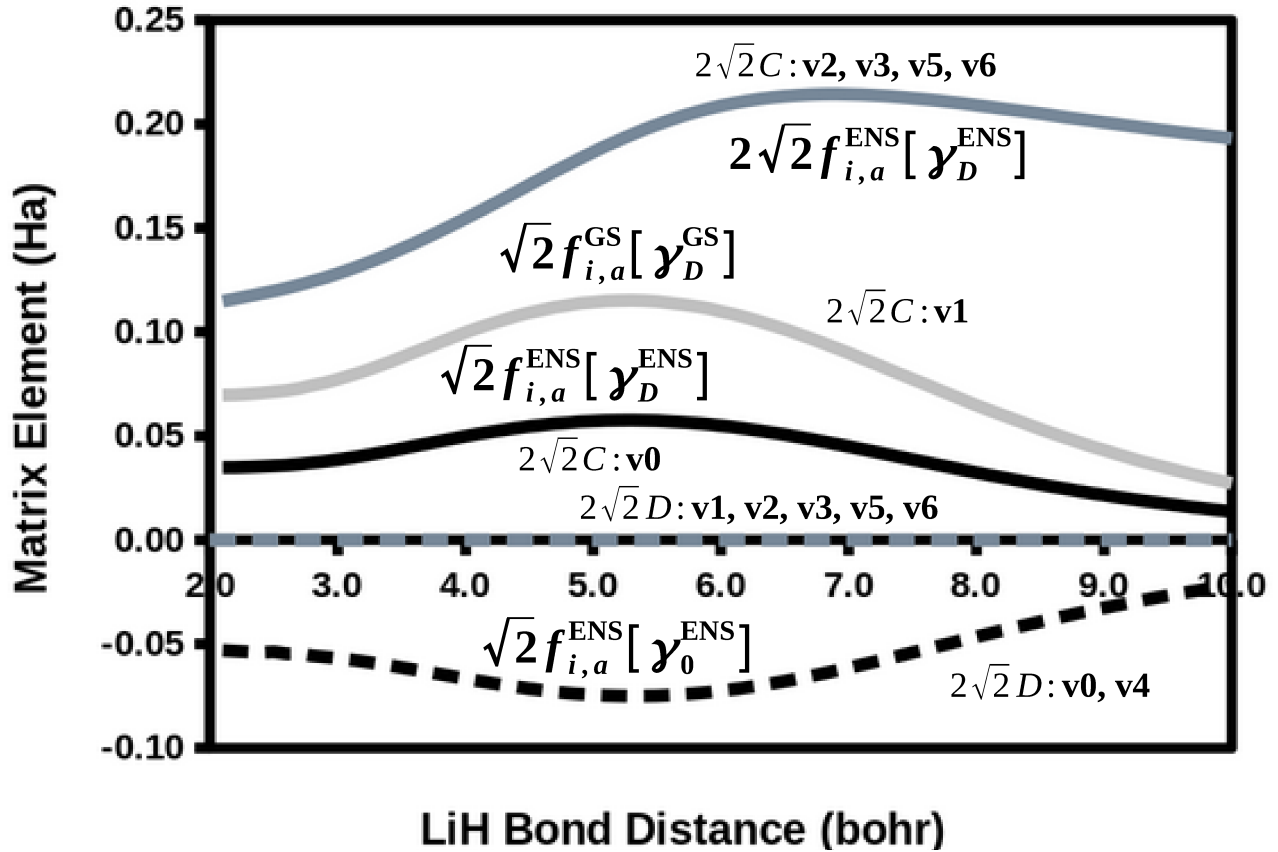


Figure 8: The coupling matrix elements used in our study as a function of bond length. (Only the variations actually discussed in the text have been indicated in the graphic.)

For the variations discussed here, $D \neq 0$ only for **v0** and **v4**. All other variations use GS MOs to describe the GS, so imposing “Brillouin’s theorem” (i.e., $D = 0$) makes sense. This means that there is no *direct* coupling between the GS SDET and the OSS SDET (GS $\not\leftrightarrow$ OSS), the coupling must pass through the DEX SDET (GS \longleftrightarrow DEX \longleftrightarrow OSS). Therefore the magnitude of the C matrix element is particularly important. The variations discussed here with $D = 0$ are **v1**, **v2**, **v3**, **v5**, and **v6**. It is also a beautiful and simplifying feature of the current theory that, except for **v1**, all the off-diagonal NOCI matrix elements are calculated with the ENS MOs as the ENS reference plays a central part in our theory. This is also not quite true in **v6** where matrix elements of \mathbf{M} and \mathbf{S} involve overlaps between GS, ENS, and DEX orbitals, but we will show that the PECs of **v6** and **v5** are nearly indistinguishable.

Figure 9 (a) shows how the excited-state MSM-LDA PECs of Article **II** (**v0**) compare with the EXACT PECs. Notice that the MSM-LDA triplet PEC is nearly superimposed with the $a^3\Sigma$ EXACT PEC. The MSM-LDA and EXACT $A^1\Sigma$ PECs are in good agreement at small bond distances but the MSM-LDA $A^1\Sigma$ PEC overestimates the EXACT $A^1\Sigma$ PEC at larger bond distances, consistent with the idea already mentioned in connection with the GS curve that the coupling matrix element is too large at longer bond distances. There is no EXACT $[\text{Li}^- \text{H}^+]$ PEC to compare with our MSM-LDA $[\text{Li}^- \text{H}^+]$ PEC. By construction, the MSM-LDA states are free of spin contamination and dissociate correctly. Nevertheless, the use of ENS MOs for describing the ground state PEC results in underbinding. Furthermore, the GS PEC has a peculiar shape which may be associated with an overestimation of the coupling matrix elements between the diabatic states. **Figure 9** (b) provides a wave-function decomposition of the **v0** $X^1\Sigma$ wave function. As expected, the character of the $X^1\Sigma$ changes from the ionic GS CSF to the biradical OSS CSF as the LiH bond is stretched. As the non-zero D matrix element provides a direct coupling between the GS and OSS CSFs, configuration mixing with the DEX configuration appears to be negligible.

Of course, the GS MOs are variationally optimized for the lowest state, meaning that the use of ENS MOs to construct the GS CSF is questionable. If we follow the analogy of conventional CI, we would normally construct all of the CSFs from the GS MOs. This is **v1**. For the C and D matrix elements, we use

$$\begin{aligned} C &= f_{i,a}^{\text{GS}}[\gamma_D^{\text{GS}}] \\ D &= f_{i,a}^{\text{GS}}[\gamma_0^{\text{GS}}] = 0, \end{aligned} \tag{36}$$

where $f_{i,a}^{\text{GS}}$ is the off-diagonal element of the KS orbital hamiltonian matrix calculated in the GS MO basis set. The expression for D is the DFT analogue of Brillouin’s theorem in wave-function theory.

Figure 10 (a) shows a comparison of the **v1** MSM-LDA PECs with the EXACT PECs. The avoidance of the diabatic curves is much too large in **Fig. 10** (a), indicating that either C is too large or that the diabatic PECs are too close in energy, or both. The wave function decomposition of the **v1** diag MSM-LDA ground state is shown in **Fig. 10**(b). We emphasize that there is no *direct* coupling between the GS SDET and the open-shell singles (OSS) SDET (GS $\not\leftrightarrow$ OSS) because $D = 0$, so the coupling must pass through the doubly excited (DEX) SDET (GS \longleftrightarrow DEX \longleftrightarrow OSS). However **Fig. 10**(b) shows the expected result that the GS CSF is important at the equilibrium geometry. However we also expect the OSS CSF to dominate at large R without significant contribution from the DEX CSF. Instead, while **Fig. 10** (b) shows that the largest contribution at large R is from the OSS CSF, the DEX CSF contribution is very significant at large R , which is counter to chemical intuition that we should be generating an OSS diradical.

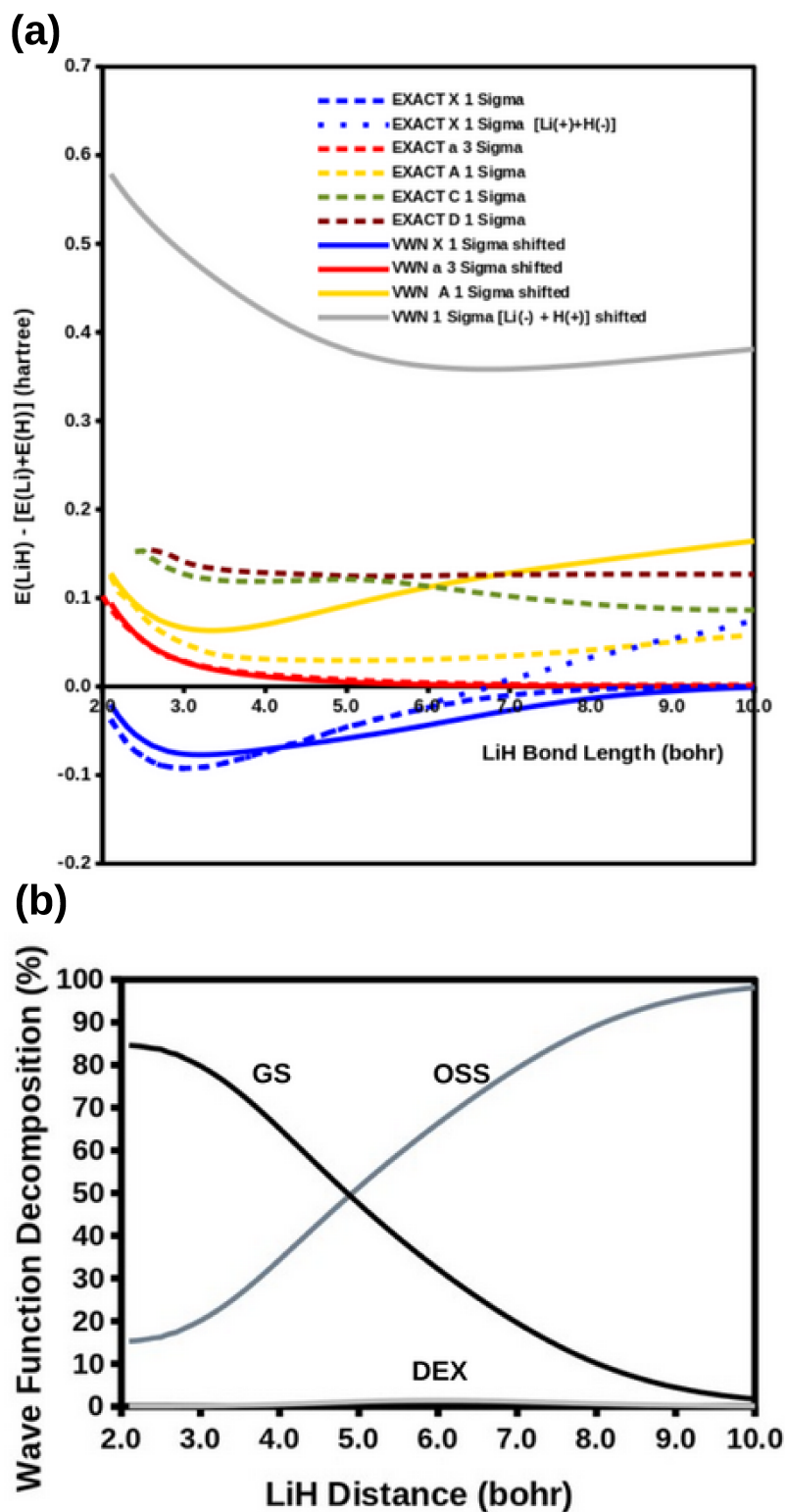


Figure 9: (a) Comparison of EXACT and MSM-LDA ($\mathbf{v0}$) PECs with the energy shifted so that the $a^3\Sigma$ curve goes to zero at $R = 10.0$ bohr. (b) Wave-function decomposition of the $\mathbf{v0}$ MSM-LDA ground state.

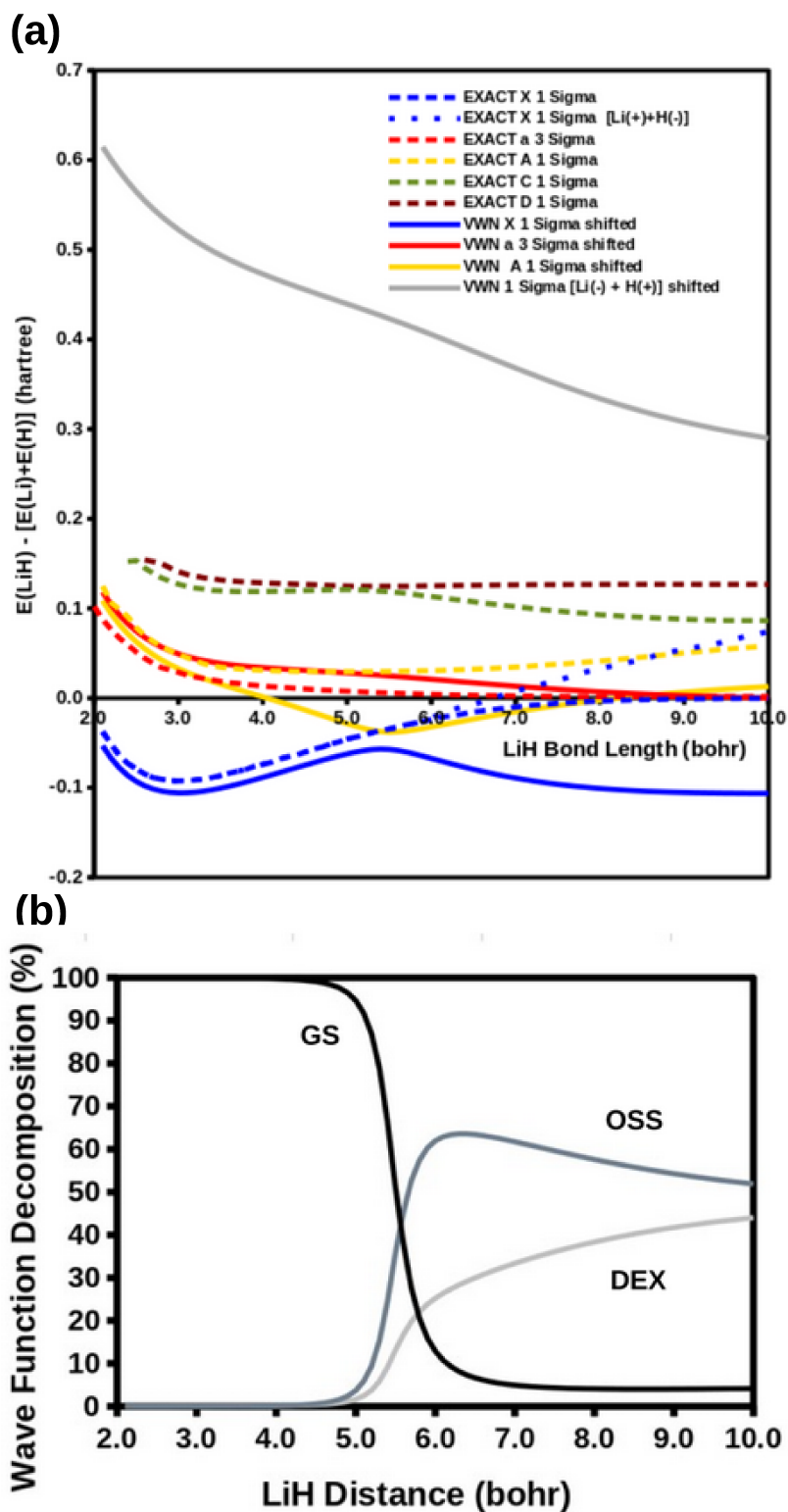


Figure 10: (a) Comparison of EXACT and ν 1 MSM-LDA PECs with the energy shifted so that the $a^3\Sigma$ curve goes to zero at $R = 10.0$ bohr. (b) Wave-function decomposition of the ν 1 MSM-LDA ground state.

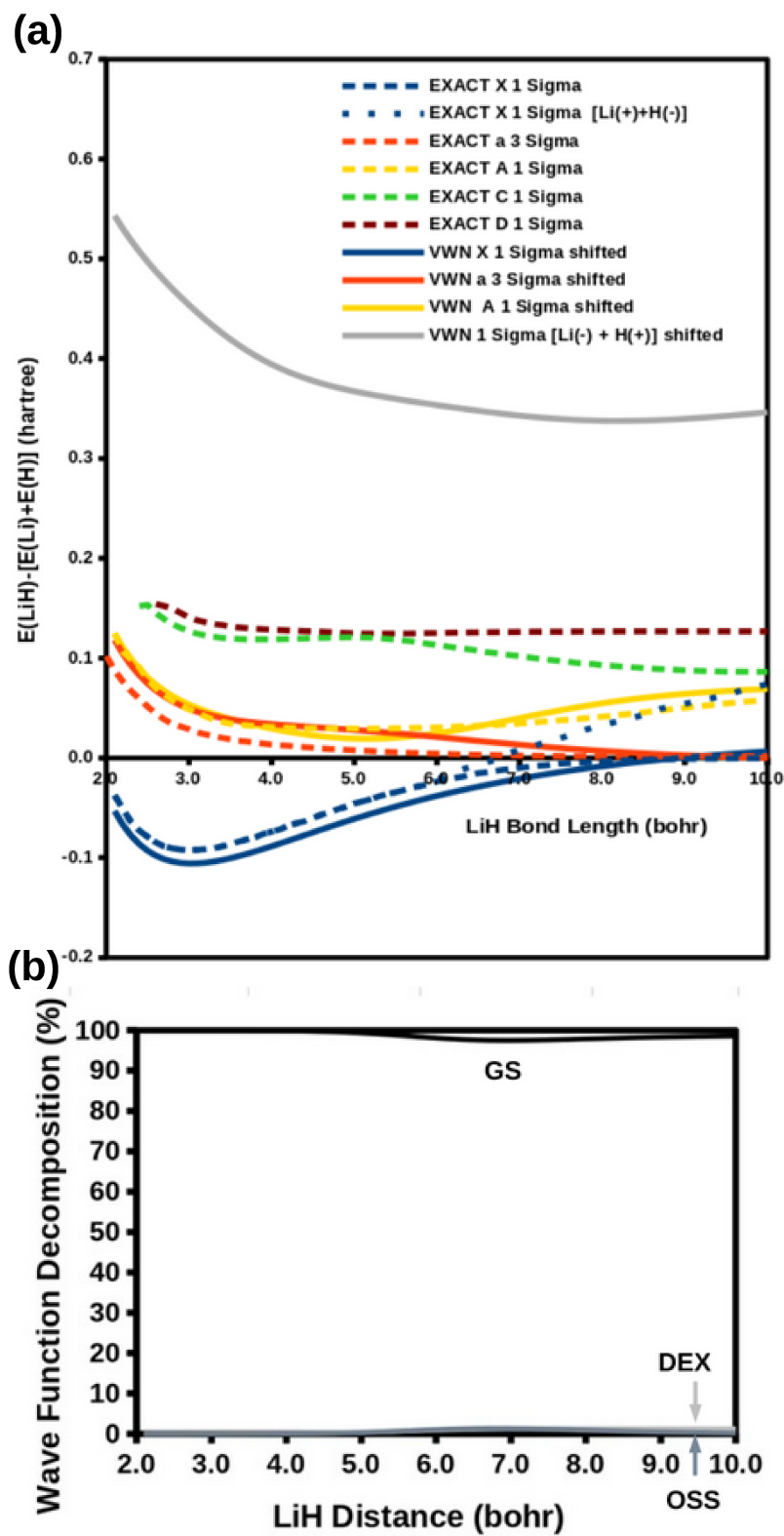


Figure 11: (a) Comparison of EXACT and $\mathbf{v3}$ MSM-LDA PECs with the energy shifted so that the $a^3\Sigma$ curve goes to zero at $R = 10.0$ bohr. (b) Wave-function decomposition of the $\mathbf{v3}$ MSM-LDA ground state.

It was argued in Sec. 3 that the C matrix element could also be approximated by using,

$$\begin{aligned} C &= 2f_{i,a}^{\text{ENS}}[\gamma_{\text{DEX}}^{\text{ENS}}] \\ D &= 0 \end{aligned} \tag{37}$$

[same as Eq. (11)]. This gives us **v2** whose PECs are not shown because it showed a collapse of the $^1\Sigma$ [$\text{Li}^- + \text{H}^+$] PEC in that the energy is 0.14 Ha at $R = 10$ bohr, rather than the expected 0.35 Ha. This caused us to move onto **v3** where the DEX determinant is calculated with DEX MOs. This fixed the problem because the [$\text{Li}^- + \text{H}^+$] PEC now has the value of 0.35 Ha at $R = 10$ bohr, giving us the best overall results for the *singlet* curves as shown in **Fig. 11** (a). However the *triplet* PEC has collapsed a bit, consistent with the previous observation that calculating the triplet PEC with MSM DFT and the ENS reference seems to be optimal. Nevertheless the wave-function decomposition of **v3** shown in Fig. 11 (b) is completely nonintuitive!

Using the GS MOs to construct the GS CSF, the ENS MOs to construct the triplet and OSS CSF, and the DEX MOs to construct the DEX CSF gives **v4**. Comparing **Fig. 12** (a) with Fig. 9 (a), shows qualitative similarities though **v0** offers a better description of the $X^1\Sigma$ PEC than does **v4** and **v4** offers a better description of the $A^1\Sigma$ PEC than does **v0**. In fact, **v4** offers a much more convincing assignment of the calculated second excited state with $A^1\Sigma$ than does **v0**. The wave-function decomposition shown in Fig. 12 (b) is also very similar to that of Fig. 9 (b)

Of the other possibilities that we tried, **v5** is the most interesting and serendipitous variant. It is identical to **v4** except that we used Eq. (37) rather than

$$\begin{aligned} C &= f_{i,a}^{\text{ENS}}[\gamma_{\text{DEX}}^{\text{ENS}}] \\ D &= f_{i,a}^{\text{ENS}}[\gamma_{\text{GS}}^{\text{ENS}}] \end{aligned} \tag{38}$$

[same as Eq. (10)]. As shown in **Fig. 13** (a), there is now a marked improvement in the calculated $X^1\Sigma$ PEC. Furthermore, the wave-function decomposition of this state shown in Fig. 13 (b) is much more physical. That is, it begins dominated by the GS CSF at the equilibrium geometry and then switches to being dominated by the OSS CSF at large R . Since coupling between the GS CSF and OSS CSF is indirect and must pass through the DEX CSF, we expect some contribution from the DEX CSF in the avoided crossing region and this is exactly what we see.

Our initial intent was to do NOCI by solving $\mathbf{H}'\vec{C}'_I = \mathbf{E}\mathbf{S}'\vec{C}'_I$. However we soon realized that this gives us the same PECs as does solving $\mathbf{H}\vec{C}'_I = \mathbf{E}\vec{C}'_I$ because \mathbf{M}^\dagger is invertible. But we also showed that $\mathbf{S}' \approx \mathbf{S}$, so it is interesting to check what happens if we replace \mathbf{S}' with the more exact \mathbf{S} and solved $\mathbf{H}'\vec{C}'_I = \mathbf{E}\mathbf{S}\vec{C}'_I$. This is what we call **v6**. As comparison of **Fig. 14**(a) with Fig. 13(a) shows, there is no noticeable difference in PECs between **v5** and **v6**. Closer comparison of the two GS PECs with the EXACT GS PEC (not shown) reveals **v5** and **v6** give nearly identical results, but that **v6** is ever so slightly worse than **v5**, so we recommend **v5** is preferred for accurate calculations and for the simplicity and internal consistency of the model.

In contrast to the computed PECs, the wave function decomposition shown in Figs. 13(b) and 14(b) and (c) do show significant differences. Of course, these differences are only important for interpretation, but the interpretation of the curves is part of what has been driving our development of diag MSM DFT. In comparing Fig. 13(b) and Fig. 14(b), we are comparing $\vec{C}'_{\text{GS}} = \mathbf{M}\vec{C}_{\text{GS}}$ with $\vec{C}''_{\text{textGS}} = \mathbf{S}^{+1/2}\vec{C}_{\text{GS}}$. The replacement of \mathbf{M} with $\mathbf{S}^{+1/2}$ is difficult to justify, but there are qualitative similarities between the graphs. A better comparison is between Fig. 13(b) and the Chirgwin-Coulson analysis shown in Fig. 14(c). Chirgwin-Coulson analysis [23] was specifically developed for NOCI. This type of analysis is briefly reviewed in the SI where it may be seen to be very similar to Mulliken population analysis. While it has the advantage of ease of application, it shares the problem of

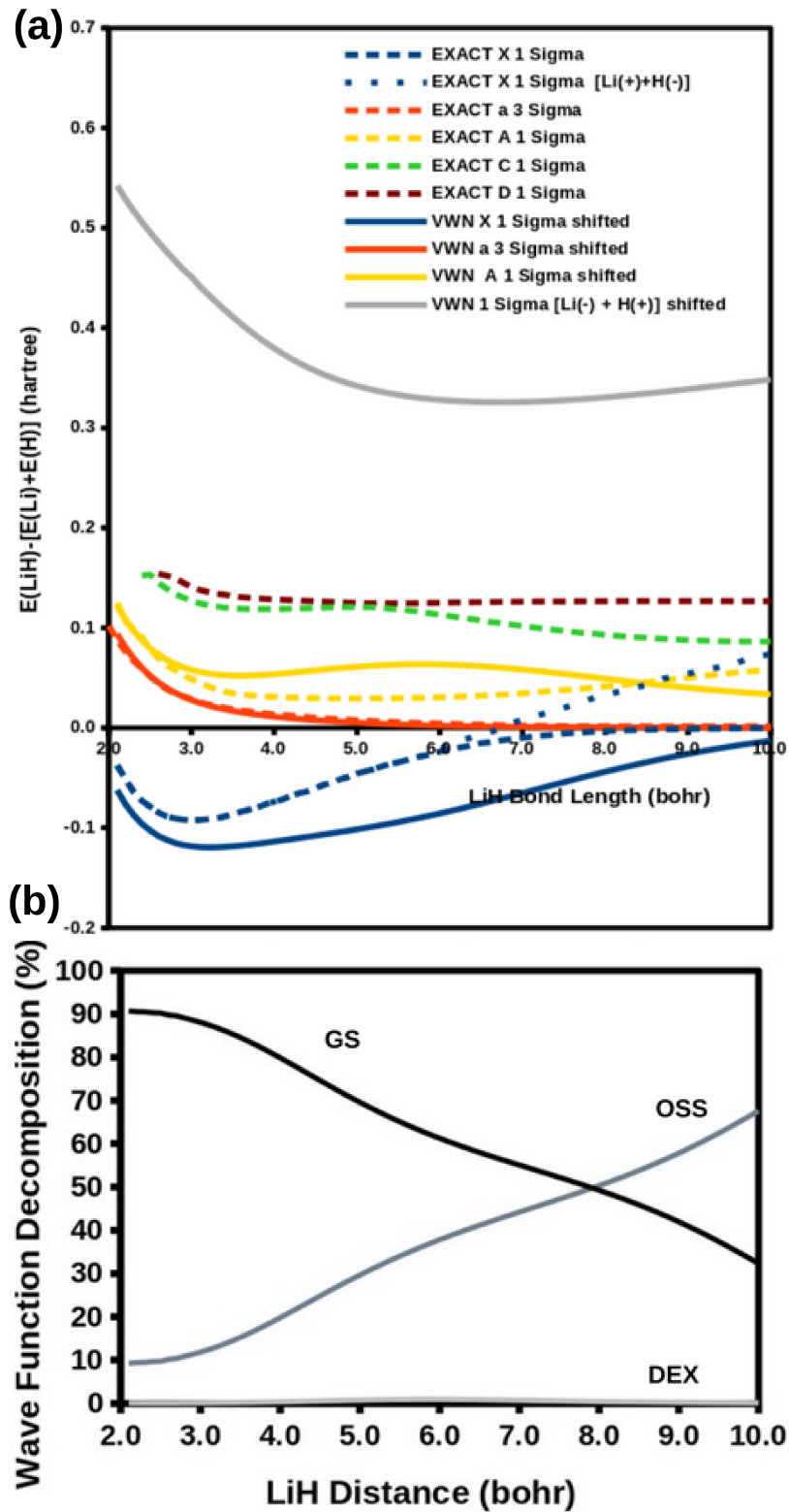


Figure 12: (a) Comparison of EXACT and v4 MSM-LDA PECs with the energy shifted so that the $a^3\Sigma$ curve goes to zero at $R = 10.0$ bohr. (b) Wave-function decomposition of the v4 MSM-LDA ground state.

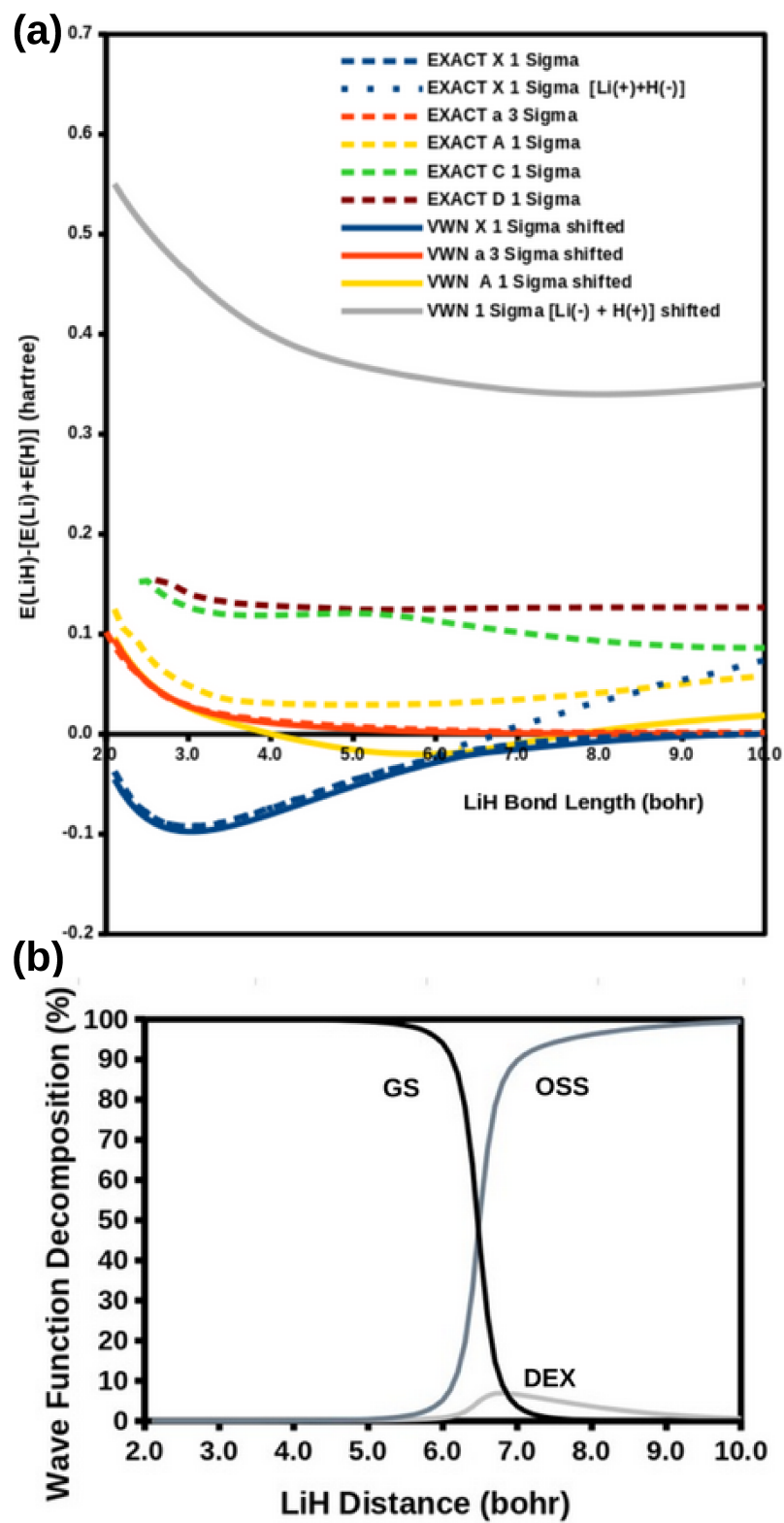


Figure 13: (a) Comparison of EXACT and $\mathbf{v5}$ MSM-LDA PECs with the energy shifted so that the $a^3\Sigma$ curve goes to zero at $R = 10.0$ bohr. (b) Wave-function decomposition of the $\mathbf{v5}$ MSM-LDA ground state.

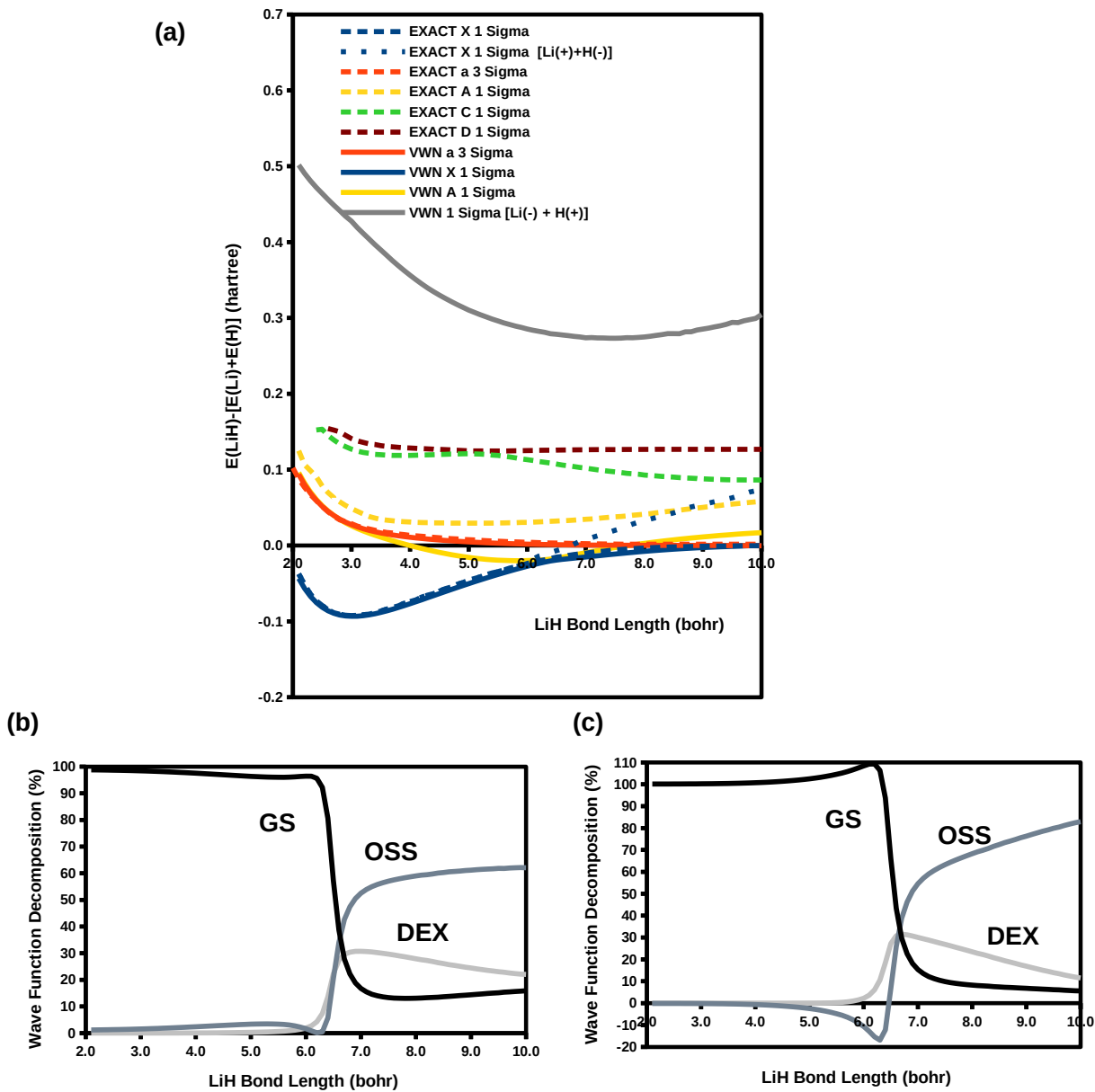


Figure 14: (a) Comparison of EXACT and v_6 MSM-LDA PECs with the energy shifted so that the $a^3\Sigma$ curve goes to zero at $R = 10.0$ bohr. Wave-function decomposition of the v_6 MSM-LDA ground state: (b) $|C_{\text{GS}}'''|^2 \times 100\%$, (c) Chirgwin-Coulson analysis.

Mulliken population analysis that component populations can become negative while others exceed 100% in order to maintain a total population of 100%. This is clearly seen in Fig. 14(c). Nevertheless, Fig. 14(c) is in better qualitative agreement with Fig. 13(b) than is Fig. 14(b).

It is now useful to realize that the goal of NOCI is *not* typically to obtain excited states, but rather to use excited states as a way to improve the ground-state PEC. *To the extent that we accept this point of view, we have succeeded in finding a relatively simple SODS MDET DFT formalism which gives a ground-state PEC close to the usual broken-symmetry (BS) DODS DFT PEC without the spin-contamination and triplet instability associated with a broken-symmetry DODS calculation.* This remarkable point is emphasized in **Fig. 15**. Here the PECs have been shifted to agree with the EXACT GS PEC at 3.8 bohr so that we may concentrate on the *shape* of the PECs. Part (a) of the figure shows that the BS PEC is a little uneven at the Coulson-Fischer (symmetry-breaking) point located at distance **A**. The calculations here are often a bit difficult to converge for technical reasons. In order to understand distance **B**, the reader is referred back to Fig. 1. Beyond this distance it may be necessary to include interactions with the Li($2p_z$)+H($1s$) diabatic curve in order to get accurate results, but this is beyond the TOTEM that we are using. Part (b) of the figure is showing the difference between the approximate and EXACT PECs. Since the EXACT PECs were digitized, the curves are a bit wiggly. Nevertheless it is clear that the two approximate curves are nearly identical in shape up to the Coulson-Fischer point **A** and errors remain small ($0.00200 \text{ Ha} = 1.26 \text{ kcal/mol}$) until point **B** where errors increase for both approximate PECs. After point **B**, errors in $\mathbf{v5}$ are larger than those in the BS calculation, but they are still small and there is neither convergence difficulty nor known slope discontinuities in the $\mathbf{v5}$ approximation. This is certainly very encouraging since our long-range goal is to go on and do response theory calculations of excited states that could be used in photochemical dynamics.

We will not show results from the other variants that we tested. They had their place in building our understanding and in convincing ourselves that we had at least tried the most obvious approaches. Because of these other calculations, we have been able to identify and present only our most interesting and informative results.

6 Concluding Discussion

In quantum chemistry, it is common to divide correlation into (“weak”) dynamic correlation and “strong” correlation, where strong correlation is further divided into static (“degenerate”) and non-dynamic (“quasidegenerate”) correlation [4]. Most density-functional approximations (DFA) used in (approximate) density-functional theory (DFT) include dynamic correlation but not strong correlation. This means that practical DFT calculations cannot describe spin- (and spatial-) multiplets nor can they be expected to describe bond breaking and formation correctly as these are processes where quasidegenerate single-determinant (SDET) energies become quasidegenerate. Hence there is a need for multideterminant (MDET) DFT methods. Especially valuable are MDET DFT methods which require no reparameterization when using different DFAs and which avoid symmetry breaking (which can be problematic in response theory calculations). We have been slowly developing what we believe to be a novel approach to MDET DFT which we call diagrammatic (diag) multiplet sum method (MSM) DFT. As explained in Article **I**, diag MSM DFT is a hybrid DFT/WFT theory method in which a small configuration interaction (CI) matrix problem is constructed in which off-diagonal CI matrix elements are obtained as educated guesses through comparison of the structure of CI matrix element (CIME) diagrams with DFT expansions. A weakness of the method is that the educated guesses must be tested numerically to see which are the most reliable. However we would like to believe that building up of this type of empirical experience can lead to a reliable, parameter-free,

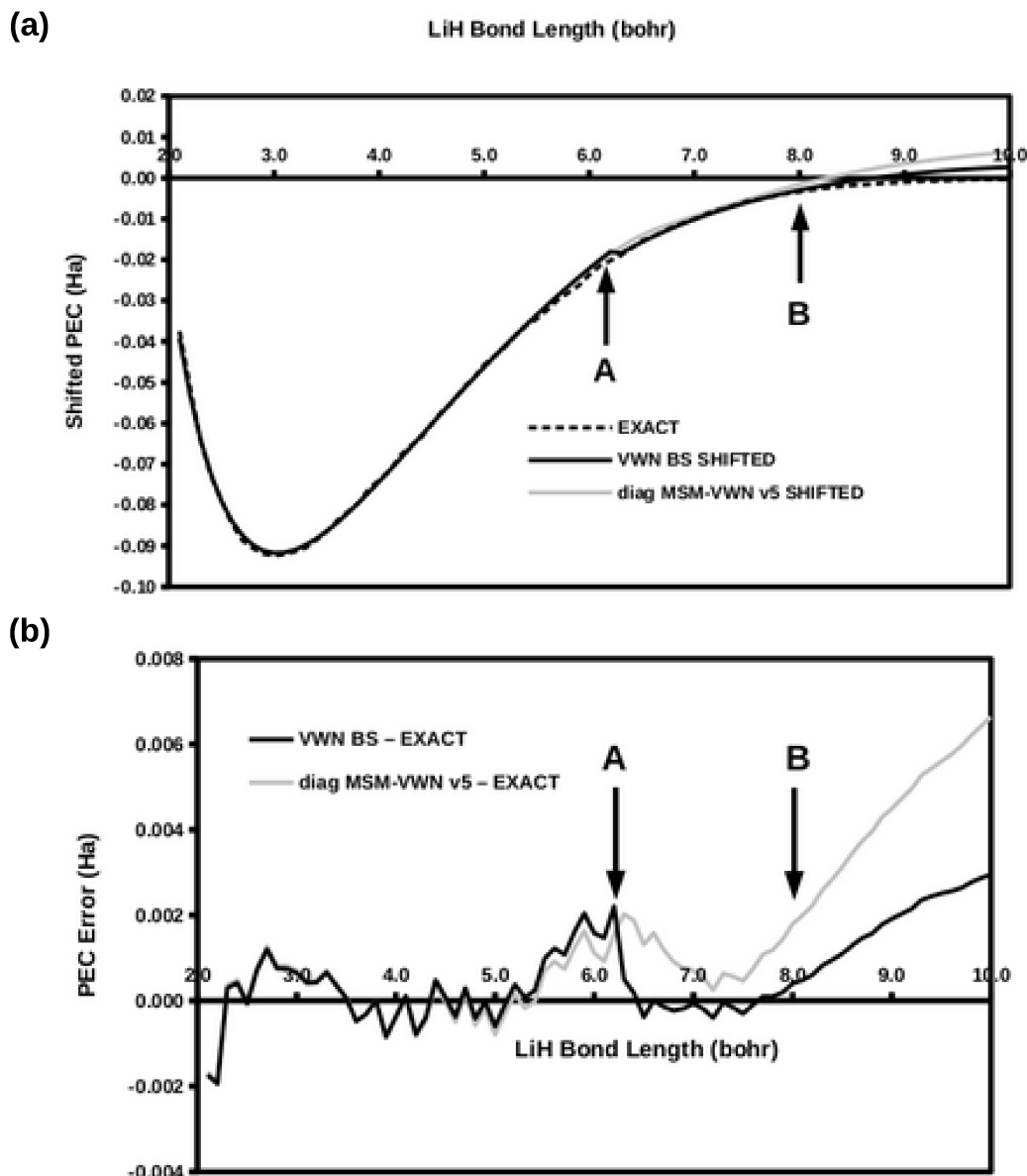


Figure 15: Comparison of BS and $\mathbf{v5}$ MSM-LDA GS shifted PECs with the EXACT GS PEC. The BS and $\mathbf{v5}$ MSM-LDA GS PECs have been shifted to have the same value as the EXACT GS PEC at 3.8 bohr: (a) EXACT, BS, and $\mathbf{v5}$ MSM-LDA GS PECs and (b) BS-EXACT and $\mathbf{v5}$ -EXACT energy difference.

same-orbital-for-different-spin (SODS) method for calculating the lowest energy potential energy surface in chemical systems. So far tests have been limited to the two-orbital two-electron model (TOTEM) as applied to H_2 , O_2 , and LiH . Article **II** showed how charge transfer could be included in diag MSM DFT in a simple fashion. But the method failed to be quantitative for the lowest energy state because it failed to include important molecular orbital (MO) relaxation effects. In this article, we have shown how relaxation effects may be incorporated into TOTEM calculations of the $X^1\Sigma$ potential energy curve (PEC) of LiH in such a way that the resultant PEC is roughly as good as that obtained by using broken symmetry (BS) with different-orbitals-for-different-spins (DODS). This is done using a small non-orthogonal CI (NOCI) calculation. In this calculation, the “excited states” are fictitious in so far as they provide, at best, only approximate descriptions of real excited states. However they are key to improving the lowest energy PEC. We find these results highly promising and believe that our ideas can help not only our efforts but also those of others working on developing MDET DFT methods. *We emphasize that, however well or badly this method proves to work for other molecules, that it is already very interesting to have found such a simple model that works so well for calculating an accurate GS PEC for LiH .*

Of course, much more extensive testing on a variety of molecules will be necessary before we can be truly confident that this is a robust method. So far, our work has been done almost entirely with a freely downloadable version of the DEMON2K program on our laptop computers and a series of simple home-made PYTHON codes. (Only one small modification was made in the DEMON2K code in the present work in order to guarantee SODS without any broken symmetry, although this modification has only a tiny effect on the final results.) The next step will be to automate the calculations within a private version of the DEMON2K code so that we can test the method for more functionals, basis sets, and other single σ bonded diatomic molecules for which we expect the TOTEM to be valid.

Supplementary Information

The SI for this article contains:

1. Author Contributions
2. Computational Details
3. Origin of the Form of the C and D Matrix Elements
4. Chirgwin-Coulson analysis

Acknowledgements

This is the continuation of a project initiated at the African Schools on Electronic Structure Methods and Applications (ASESMA) that took place in Accra, Ghana, in 2025. We thank Lynn Scherwood Nkeme for helpful discussions about this project at ASESMA 2025. MEC thanks Kim C. Casida for helpful discussions regarding the presentation of our results.

References

- [1] P. Hohenberg and W. Kohn, [Inhomogenous electron gas](#), Phys. Rev. **136**, B864 (1964).

- [2] W. Kohn and L. J. Sham, [Self-consistent equations including exchange and correlation effects](#), Phys. Rev. **140**, A1133 (1965).
- [3] A. Seidl, A. Görling, P. Vogl, and J. A. Majewski, [Generalized Kohn-Sham scheme and the band gap problem](#), Phys. Rev. B **53**, 3764 (1996).
- [4] R. J. Bartlett and J. F. Stanton, [Applications of post-Hartree-Fock methods: A tutorial](#), in *Reviews in Computational Chemistry, Vol. 5*, edited by K. B. Lipkowitz and D. B. Boyd, page 65, VCH Publishers, New York, 1994.
- [5] J. P. Perdew, R. G. Parr, M. Levy, and J. L. Balduz, [Density-functional theory for fractional particle number: Derivative discontinuities of the energy](#), Phys. Rev. Lett. **49**, 1691 (1982).
- [6] L. J. Sham and M. Schlüter, [Density-functional theory of the energy gap](#), Phys. Rev. Lett. **51**, 1888 (1983).
- [7] J. Perdew, [What do the Kohn-Sham orbital energies mean? How do atoms dissociate?](#), in *Density Functional Methods in Physics*, edited by R. M. Dreizler and J. da Providência, page 265, Plenum, New York, 1985.
- [8] O. V. Gritsenko and E. J. Baerends, [Effect of molecular dissociation on the exchange-correlation Kohn-Sham potential](#), Phys. Rev. A **54**, 1957 (1996).
- [9] D. G. Tempel, T. J. Martínez, and N. T. Maitra, [Revisiting molecular dissociation in density functional theory: A simple model](#), J. Chem. Theory Comput. **5**, 770 (2009).
- [10] M. E. Casida, F. Gutierrez, J. Guan, F. Gadea, D. R. Salahub, and J. Daudey, [Charge-transfer correction for improved time-dependent local density approximation excited-state potential energy curves: Analysis within the two-level model with illustration for H₂ and LiH](#), J. Chem. Phys. **113**, 7062 (2000).
- [11] E. Tapavicza, I. Tavernelli, U. Rothlisberger, C. Filippi, and M. E. Casida, [Mixed time-dependent density-functional theory/classical surface hopping study of oxirane photochemistry](#), J. Chem. Phys. **129**, 124108 (2008).
- [12] A. D. Becke, [Perspective: Fifty years of density-functional theory in chemical physics](#), J. Chem. Phys. **140**, 18A301 (2014).
- [13] R. J. Bartlett, [Ab initio DFT and its role in electronic structure theory](#), Mol. Phys. **108**, 3299 (2010).
- [14] T. Ziegler, A. Rauk, and E. J. Baerends, [On the calculation of multiplet energies by the Hartree-Fock-Slater method](#), Theor. Chim. Acta **4**, 877 (1977).
- [15] C. Daul, [Density functional theory applied to the excited states of coordination compounds](#), Int. J. Quantum Chem. **52**, 867 (1994).
- [16] A. Ponra, A. J. Etindele, O. Motapon, and M. E. Casida, [Practical treatment of singlet oxygen with density-functional theory and the multiplet-sum method](#), Theo. Chem. Acc. **140**, 154 (2021).
- [17] A. Ponra, C. Bakasa, A. J. Etindele, and M. E. Casida, [Diagrammatic multiplet-sum method \(MSM\) density-functional theory \(DFT\): Investigation of the transferability of integrals in "simple" DFT-based approaches to multi-determinantal problems](#), J. Chem. Phys. **159**, 244306 (2023).

- [18] M. E. Casida, A. Ponra, C. Bakasa, and A. J. Etindele, [Diagrammatic multiplet-sum method \(MSM\) density-functional theory \(DFT\): Completion of the two-orbital two-electron model \(TOTEM\) with an application to the avoided crossing in lithium hydride \(LiH\)](#), *J. Chem. Phys.* **162**, 144317 (2025).
- [19] F. X. Gadéa and T. Leininger, [Accurate *ab initio* calculations for LiH and its ions LiH⁺ and LiH⁻](#), *Theor. Chem. Acc.* **116**, 566 (2006).
- [20] A. Rohatgi, [WEBPLOTDIGITIZER](#), <https://automeris.io/>, Last accessed 18 February 2026.
- [21] B. Schaftenaar, [MOLDEN: A pre- and post processing program of molecular electronic structure](#), <https://www3.cmbi.umcn.nl/molden/>, Last accessed 22 May 2021.
- [22] Y. Lu and J. Gao, [Multistate density functional theory: Theory, methods, and applications](#), *WIREs Comput. Mol. Sci.* **15**, e70043 (2025).
- [23] B. H. Chirgwin and C. A. Coulson, [The electronic structure of conjugated systems. VI.](#), *Proc. Roy. Soc. Lond. A* **201**, 196 (1950).
- [24] L. H. Sarett, [Research and invention](#), *Proc. Natl. Acad. Sci. USA* **80**, 4572 (1983).